

Robustifying Vision Transformer without Retraining from Scratch by Test-Time Class-Conditional Feature Alignment

Takeshi Kojima*, Yutaka Matsuo and Yusuke Iwasawa

The University of Tokyo, Japan

{t.kojima,matsuo,iwasawa}@weblab.t.u-tokyo.ac.jp

Abstract

Vision Transformer (ViT) is becoming more popular in image processing. Specifically, we investigate the effectiveness of test-time adaptation (TTA) on ViT, a technique that has emerged to correct its prediction during test-time by itself. First, we benchmark various test-time adaptation approaches on ViT-B16 and ViT-L16. It is shown that the TTA is effective on ViT and the prior-convention (sensibly selecting modulation parameters) is not necessary when using proper loss function. Based on the observation, we propose a new test-time adaptation method called class-conditional feature alignment (CFA), which minimizes both the class-conditional distribution differences and the whole distribution differences of the hidden representation between the source and target in an online manner. Experiments of image classification tasks on common corruption (CIFAR-10-C, CIFAR-100-C, and ImageNet-C) and domain adaptation (digits datasets and ImageNet-Sketch) show that CFA stably outperforms the existing baselines on various datasets. We also verify that CFA is model agnostic by experimenting on ResNet, MLP-Mixer, and several ViT variants (ViT-AugReg, DeiT, and BeiT). Using BeiT backbone, CFA achieves 19.8% top-1 error rate on ImageNet-C, outperforming the existing test-time adaptation baseline 44.0%. This is a state-of-the-art result among TTA methods that do not need to alter training phase.¹

1 Introduction

Inspired by the success in natural language processing, Transformer [Vaswani *et al.*, 2017] is becoming more and more popular in various image processing tasks, including image recognition [Dosovitskiy *et al.*, 2020; Touvron *et al.*, 2021], object detection [Carion *et al.*, 2020], and video processing [Zhou *et al.*, 2018; Zeng *et al.*, 2020]. Notably, [Dosovitskiy *et al.*, 2020] proposed Vision Transformer (ViT),

which adapts Transformer architecture to image classification tasks and shows that it achieves comparable or superior performance to that of the conventional convolutional neural networks (CNNs). Follow-up research also shows that ViT is more robust to the common corruptions and perturbations than convolution-based models (e.g., ResNet) [Paul and Chen, 2021; Morrison *et al.*, 2021], which is an important property for safety-critical applications.

This study seeks to answer the following question: *can we improve the robustness of ViT without retraining it from scratch?* Most prior works focused on how to robustify the models during training. For example, [Hendrycks *et al.*, 2019; Hendrycks *et al.*, 2020] demonstrated that several data augmentation improves robustness of convolutional neural networks (CNN). Similarly, [Chen *et al.*, 2022] shows that a sharpness-aware optimizer improves the robustness of ViT. Unfortunately, such approaches require retraining the models from scratch, which entails a massive computational burden and training time for large models (such as ViT). Moreover, sometimes dataset for pre-training is not publicly available, which makes it impossible to retrain the models.

This study investigates the effectiveness of test-time adaptation (TTA) to robustify ViT. TTA is a recently emerged approach for improving the robustness of models without retraining them from scratch and accessing to training dataset [Schneider *et al.*, 2020; Nado *et al.*, 2020; Wang *et al.*, 2020]. Instead, it corrects the model’s prediction for test data by modulating its parameters during test time. For example, [Wang *et al.*, 2020] proposed Tent, which modulates the parameters of batch normalization (BN) by minimizing prediction entropy. It was shown that Tent can significantly improve the robustness of ResNet. TTA has two major advantages over usual training-time techniques. First, it does not alter the training phase and thus does not need to repeat the computationally heavy training phase. Second, it does not require accessing to the source data during adaptation, which is impossible in the case of large pre-trained models.

Conceptually speaking, TTA can be applied to arbitrary network architectures. However, naively modulating model parameters during test-time may cause a catastrophic failure as discussed in [Wang *et al.*, 2020]. To avoid the issue, prior works often limited the modulation parameters, which resulted in architecture constraints. For example, [Schneider *et al.*, 2020; Wang *et al.*, 2020] modulated statistics and/or

*Contact Author

¹Code is available at <https://github.com/kojima-takeshi188/CFA>.

affine transformation in batch normalization (BN) layer, but the BN-based method cannot be applied to some modern models such as ViT since they do not have BN.

This study contributes to addressing this research question by following two means. First, we benchmark various test-time adaptation methods on ViT using several robustness benchmark tasks (CIFAR10-C, CIFAR100-C, ImageNet-C, and several domain adaptation tasks). We also design modulation parameters potentially suitable for ViT-based architectures. The tested methods include entropy minimization [Wang *et al.*, 2020], pseudo-classifier [Iwasawa and Matsuo, 2021], pseudo-label [Lee and others, 2013], diversity regularization [Liang *et al.*, 2020], and feature alignments [Liu *et al.*, 2021]. Regarding modulation parameters, we sweep over the following four candidates: layer normalization [Ba *et al.*, 2016], CLS token, feature extractor [Liang *et al.*, 2020], and entire parameters of a model. The results indicate that the prior convention in test-time adaptation (i.e., limiting modulation parameters) *is not necessary* when using proper loss function, while it is necessary for pure entropy minimization based approach. This observation is important for applying TTA to arbitrary network architectures.

We then propose a new loss function: test-time class-conditional feature alignment (CFA). Our approach can be categorized into feature alignment approach as with [Liu *et al.*, 2021], which minimize the gap of the statistics between training and test domain. It is worth noting that the feature alignment approach for test-time adaptation (e.g., our approach and [Liu *et al.*, 2021]) assumes that one can access to the statistics on the source dataset during the test phase but does not need to access to the source dataset itself and to repeat the computationally heavy training². Therefore, this approach can be used without source dataset during adaptation. We show that such complementary information about the source data distribution can stabilize the training without selecting the modulation parameters. In addition, we extend the feature alignment approach [Liu *et al.*, 2021] by the following two means. First, CFA aligns class-conditional statistics as well as the statistics of overall distribution. Second, we calculate the statistics after properly normalizing the hidden representations. Despite the simplicity, these techniques significantly boost the performance of test-time adaptation.

In summary, our main contributions are as follows.

- This is the first study that verifies the effectiveness of test-time adaptation methods on ViT. By benchmarking several test-time adaptation approaches under common corruptions and domain adaptation tasks, we have validated that the robustness of ViT model is improved during test time without retraining the model from scratch.
- We introduce a new test-time adaptation method (CFA). Throughout the experiment, CFA achieves better results

²Test-time adaptation generally assumes that the model would be distributed without source data due to bandwidth, privacy, or profit reasons [Wang *et al.*, 2020]. We argue that the statistics of source data would be distributed even in such a situation since it could drastically compress data size and eliminate sensitive information. In fact, some layers often used in typical neural networks contain statistics of source data (e.g., batch normalization)

than existing baselines on multiple datasets. In addition, CFA is robust to hyperparameter tuning, which is important in practically setting up test-time adaptation.

- We show that CFA consistently improves the robustness on a wide variety of backbone networks during test time. In particular, we achieve the state-of-the-art results of test-time adaptation on ImageNet-C with a 19.8 % top-1 error rate when using BeiT-L16 as a backbone network.

2 Related Work

2.1 Vision Transformer (ViT)

Transformer [Vaswani *et al.*, 2017], first proposed in natural language processing (NLP) field, also achieves great performance in image processing as Vision Transformer (ViT) [Dosovitskiy *et al.*, 2020]. ViT divides input image data into small patches and translates them to embedding vectors, otherwise known as a "token". Extra learnable class embedding (CLS token) is added to the sequence of the tokens before feeding them into Transformer Encoder. Transformer Encoder mainly consists of multilayered global self-attention blocks and MLP blocks. The blocks include layer normalization [Ba *et al.*, 2016] as one function. An MLP head is added to top layer of the CLS token as a classifier.

Since its invention, ViT has rapidly become popular in the field of computer vision. Many applications and extensions have been proposed thus far. For example, [Touvron *et al.*, 2021],[Bao *et al.*, 2021], and [Steiner *et al.*, 2021] showed that the performance of ViT is respectively improved by distillation (DeiT), self-supervised learning (BeiT), and data augmentation (ViT-AugReg) during pre-training phase. More recently, [Tolstikhin *et al.*, 2021] proposed MLP-Mixer, which was proven to be quite competitive with ViT by replacing self-attention blocks with MLP layers.

This study is interested in how to robustify ViT to the common perturbations. Recent experimental research has verified that ViT inherently has robustness without any adaptation or any additional data augmentation. Several studies empirically show that ViT is inherently more robust than CNNs [Paul and Chen, 2021; Morrison *et al.*, 2021; Naseer *et al.*, 2021; Yamada and Otani, 2022] by using some benchmark datasets. Several studies have shown that the robustness of ViT can be improved by changing the training strategy, such as using a larger data set for the pre-training phase [Paul and Chen, 2021; Bhojanapalli *et al.*, 2021] or a sharpness-aware optimizer for the training phase [Chen *et al.*, 2022]. However, retraining such a massively pre-trained model from scratch is not desirable considering the computational burden. The larger the data and model, the higher it costs for retraining. At the same time, however, the model size also matters for robustness, i.e., larger models tend to be more robust by themselves (See Appendix E for the detail). This observation motivated us to investigate a lightweight and model-agnostic way to improve the robustness of the models.

2.2 Test-Time Adaptation (TTA)

This study investigates the effectiveness of the test-time adaptation approaches for Vision Transformer and its variants. Unlike most existing works that focus on training phase to

improve the robustness, test-time adaptation focuses on test-time. In other words, test-time adaptation does not alter the training phase; therefore, we do not need to repetitively run computationally heavy training to improve robustness.

The algorithm of existing test-time adaptation can be summarized by following two aspects: (1) adaptation function f_{adapt} and (2) modulation parameters ψ . Literally, f_{adapt} is a function that determines how to modulate the model parameter during the test time. More formally, f_{adapt} receives a batch of unlabeled images X_{test} , which is available online at test-time, and updates the target parameter ψ using the data. A naive instance of f_{adapt} might use stochastic gradient descent (SGD) by designing a loss function that can effectively incorporate X_{test} to correct its prediction. For example, Tent [Wang *et al.*, 2020], which is a pioneering method for test-time adaptation, minimizes prediction entropy using SGD, based on the assumption that a more confident prediction (i.e. low prediction entropy) leads to a more accurate prediction. One can also use different loss functions (such as pseudo-label (PL) [Lee and others, 2013], diversity regularization (SHOT-IM) [Liang *et al.*, 2020], and feature alignments (TFA) [Liu *et al.*, 2021]), or design optimization-free procedures to update the model (e.g., T-BN [Schneider *et al.*, 2020; Nado *et al.*, 2020] and T3A [Iwasawa and Matsuo, 2021]).

The second aspect is the selection of modulation parameters ψ . As discussed in [Wang *et al.*, 2020], updating the entire model parameters θ is often ineffective in test-time optimization because θ is usually the only information of the source data in the setup, and updating all parameters without restriction results in catastrophic failure. (See Table 1 for the experiment result). Consequently, prior works also proposed to sensibly select modulation parameters along with the adaptation method f_{adapt} . For example, [Schneider *et al.*, 2020; Nado *et al.*, 2020] proposed to re-estimate the statistics of batch normalization [Ioffe and Szegedy, 2015] during the test time while fixing the other parameters. Similarly, Tent [Wang *et al.*, 2020] modulated only a set of affine transformation parameters of the BN layer. This causes two problems when applying test-time adaptation to ViT. First, ViT has significantly larger parameters compared to ResNet which is the standard test bed of prior studies. Consequently, the effectiveness of TTA on such a huge model has not been fully investigated. Second, ViT and its variants do not have BN, so they cannot directly take advantage of the common good strategy. In other words, there is a lack of knowledge regarding which parameter should be updated to effectively robustify ViT.

In this study, we avoid the difficulty of sensibly selecting the modulation parameters by incorporating the feature-alignment approach. More specifically, we explicitly minimize the difference between some statistics of source distribution and target (test) distribution, rather than simply modulating model parameters only given data from target distribution. In other words, we leverage the source statistics as auxiliary information regarding the source distribution to prevent adaptation from causing the aforementioned catastrophic failure. Note that our method does not rely on the co-existence of source and target data and does not violate the setting of test-time adaptation.

Similar to our work, [Liu *et al.*, 2021] recently proposed

test-time feature alignment (TFA), which aligns the hidden representation between source and target data by minimizing the distance of the mean and covariance matrix. Our method is different from TFA in the following two aspects. First, we propose to align class-conditional statistics as well as the statistics of overall distribution. Second, we propose to calculate the statistics after properly normalizing the hidden representations. In §4.4, our experiment results demonstrate that these techniques stably improve the performance of various tasks based on various backbone networks.

3 Methods

3.1 Modulation Parameters

As discussed in §2.2, the choice of modulation parameters is regarded as important in test-time adaptation but prior BN-based modulation is not applicable to Vision Transformer. To find good candidates for ψ in ViT, we sweep over the following four candidates: layer normalization [Ba *et al.*, 2016], CLS token, feature extractor parameters, and all parameters.

A Layer normalization (LN) re-estimates the mean and standard deviation of input across the dimensions of the input, followed by the affine transformation for each dimension. We update the affine transformation parameters in LN for adaptation. A CLS token is a parameterized vector and proven to be efficient for fine-tuning large models for downstream tasks in NLP [Lester *et al.*, 2021]. A feature extractor is defined as any module in a model except for its classifier. This term is borrowed from [Liang *et al.*, 2020]. In the case of ViT, its feature extractor consists of Transformer Encoder, patch embeddings, and positional embeddings. Updating feature extractor parameters is a basic unsupervised domain adaptation setting, while [Wang *et al.*, 2020] claimed that it was ineffective in test-time adaptation setup (see §2.2).

It is worth noting that these choices of modulation parameters are applicable to many modern architectures, including ViT, DeiT, MLP-Mixer, and BeiT. This property is important in practice because a better backbone network usually provides significant performance gains. We also empirically show the effectiveness of TTA on such various architectures.

3.2 Class-Conditional Feature Alignment

Regarding the adaptation function, this study proposes a new loss function, called class-conditional feature alignment (CFA). Similar to the most prior works, our method uses stochastic gradient descent to adapt the model during test-time. Unlike the prior methods such as Tent, PL, and T3A that modulate the parameters using the data available at test-time only, our method aligns the statistics of features between source and target. In other words, we leverage the source statistics as an auxiliary information regarding the source distribution to prevent the model from suffering a catastrophic failure.

Assume that a model consists of two components; a linear classifier g_ω as last layer, and a feature extractor f_ϕ before the classifier. A set of source training samples is denoted as $X^s = \{x_i^s\}_{i=1}^{N_s}$. While prior works often calculate the statistics of feature output by f_ϕ , the feature is not always normalized. For example, ViT uses GELU as an activation function

Algorithm 1 Online Adaptation using CFA

Input: Fine-tuned DNN model with parameters θ , Partial parameters to be updated during adaptation $\psi \subset \theta$, Target test dataset X^t , m -th ordered batch data $X^{t,m} \subset X^t$, Statistics of Eq.(2) (3) (4) calculated from source training dataset.

Output:

- 1: **for** $m = 1$ to M **do**
 - 2: Predict labels $\hat{Y}^{t,m}$ for $X^{t,m}$
 - 3: Calculate statistics Eq.(6) (7) (8) for $X^{t,m}$
 - 4: Update ψ using Eq.(11)
 - 5: **end for**
 - 6: **return** $(\hat{Y}^{t,1}, \dots, \hat{Y}^{t,M})$
-

and LN with elementwise affine transformation before classifier, which is not bounded. We found that this causes unstable behavior especially when matching higher order moments of distributions. Thus, before calculating the statistics, we normalize (bound the minimum and maximum value of) the hidden representation for each sample $f_\phi(x_i^s)$ as follows.

$$h(x_i^s) = \text{Tanh}(LN^\dagger(f_\phi(x_i^s))), \quad (1)$$

where LN^\dagger is defined as layer normalization *without affine transformation*. Despite the simplicity, we empirically find that not only matching higher order moment of overall distribution is stabilized, but also the performance of class-conditional feature alignment is boosted (See Table 5 for the detail). The feature normalization might have a positive effect on class-conditional distribution matching by highlighting the distribution property of each class.

After the normalization, the mean and higher order central moments of overall distribution on source data are calculated and stored in memory as fixed values.

$$\mu^s = \frac{1}{|X^s|} \sum_{x_i^s \in X^s} h(x_i^s), \quad (2)$$

$$\mathbb{M}_k^s = \frac{1}{|X^s|} \sum_{x_i^s \in X^s} (h(x_i^s) - \mu^s)^k, \quad (k = 2, \dots, K) \quad (3)$$

where K denotes the maximum number of moments. Class-conditional mean of the normalized hidden representations is also calculated and stored in memory as fixed value as follows

$$\mu_c^s = \frac{1}{|X_c^s|} \sum_{x_i^s \in X_c^s} h(x_i^s), \quad (c = 1, \dots, C) \quad (4)$$

where C denotes the number of classes. $X_c^s \subset X^s$ contains all the source samples whose ground-truth labels are c . Note that these statistics are calculated before adaptation, i.e., we do not need to access to source data itself in test phase.

CFA uses these statistics to adapt the model during test phase. Assume that a sequence of test data drawn from target distribution arrives at our model one after another. Test dataset is denoted as $X^t = \{x_i^t\}_{i=1}^{N_t}$, and a set of test data in m -th batch is denoted as $X^{t,m} \subset X^t$, ($m = 1, \dots, M$). For each batch, hidden representations of test data are normalized and their statistics are calculated in the same way as source.

$$h(x_i^t) = \text{Tanh}(LN^\dagger(f_\phi(x_i^t))), \quad (5)$$

ViT-B16	Tent	PL	SHOT-IM	CFA
LN	50.6±0.5	55.7±1.4	45.7±0.0	43.9±0.0
CLS	59.4±0.0	60.6±0.0	59.9±0.0	58.2±0.0
Feature	56.2±2.2	60.8±2.1	43.9±0.0	41.8±0.0
ALL	59.1±1.0	61.4±2.2	44.0±0.0	41.8±0.0
ViT-L16	Tent	PL	SHOT-IM	CFA
LN	42.3±0.0	44.3±0.0	42.0±0.0	40.2±0.0
CLS	50.3±0.0	51.3±0.0	50.7±0.1	49.2±0.0
Feature	43.8±0.6	46.5±0.8	38.4±0.0	36.6±0.0
ALL	44.2±1.1	46.9±0.7	38.4±0.0	36.6±0.0

Table 1: Modulation parameter choice study. The evaluation metric is top-1 error on ImageNet-C averaged over 15 corruption types with severity level of 5. ViT-B16 and ViT-L16 are used as the models. CLS: CLS token, LN: layernorm params, Feature: parameters of feature extractor, ALL: all the parameters of ViT.

$$\mu^{t,m} = \frac{1}{|X^{t,m}|} \sum_{x_i^t \in X^{t,m}} h(x_i^t), \quad (6)$$

$$\mathbb{M}_k^{t,m} = \frac{1}{|X^{t,m}|} \sum_{x_i^t \in X^{t,m}} (h(x_i^t) - \mu^{t,m})^k, \quad (k = 2 \dots K) \quad (7)$$

$$\mu_c^{t,m} = \frac{1}{|X_c^{t,m}|} \sum_{x_i^t \in X_c^{t,m}} h(x_i^t), \quad (c = 1, \dots, C) \quad (8)$$

where $X_c^{t,m}$, which is a subset of $X^{t,m}$, includes all samples in the current batch annotated as class c by pseudo-labeling $\text{argmax}_c g_\omega(f_\phi(x_i^t))$. In this study, the overall distribution distance is defined by the central moment distance (CMD) [Zellinger *et al.*, 2017] (see Appendix G for details):

$$\mathcal{L}_F = \frac{1}{2} \|\mu^s - \mu^{t,m}\|_2 + \frac{1}{2k} \sum_{k=2}^K \|\mathbb{M}_k^s - \mathbb{M}_k^{t,m}\|_2. \quad (9)$$

As for class-conditional distribution matching, following prior studies in UDA setting ([Xie *et al.*, 2018; Deng *et al.*, 2019]), we use class-conditional centroid alignment.

$$\mathcal{L}_C = \frac{1}{2|C'|} \sum_{c \in C'} \|\mu_c^s - \mu_c^{t,m}\|_2, \quad (10)$$

where C' denotes a set of the pseudo labelled classes belonging to the current target minibatch samples. The first-order moment (centroid) is sufficient for class-conditional feature alignment when class size is larger than batch size. Parameters ψ of the model are updated by the gradient of the following loss function based on the target batch data at hand.

$$\mathcal{L} = \mathcal{L}_F + \lambda \mathcal{L}_C, \quad (11)$$

where λ is a balancing hyperparameter. Following [Wang *et al.*, 2020], for efficient computation, we use the scheme that the parameter update follows the prediction for the current batch. Therefore, the update only affects the next batch. The adaptation procedure is summarized in Algorithm 1.

Method	Type	Class Cond.	C10→ C10-C	C100→ C100-C	ImageNet→ ImageNet-C	SVHN→ MNIST	SVHN→ MNIST-M	ImageNet→ ImageNet-S
Source	-		14.6±0.0	35.1±0.0	61.9±0.0	23.2±0.0	46.2±0.0	64.1±0.0
T3A	gf		13.7±0.0	34.0±0.0	61.2±0.0	17.4±0.3	40.9±0.2	61.7±0.0
Tent	fm		10.9±0.2	27.4±0.5	50.6±0.5	15.3±0.2	53.0±1.7	68.3±4.3
PL	fm		11.9±0.0	30.1±0.5	55.7±1.4	15.8±0.7	49.7±1.9	62.2±1.2
SHOT-IM	fm		8.9±0.0	25.6±0.0	45.7±0.0	13.7±0.1	36.6±0.4	56.1±0.1
TFA(-)	fa		8.8±0.0	32.2±0.2	57.8±0.1	16.5±0.1	39.3±0.4	65.7±0.2
CFA-F (Ours)	fa		8.7±0.0	25.2±0.0	46.7±0.0	16.3±0.0	39.9±0.1	57.2±0.1
CFA-C (Ours)	fa	✓	8.5±0.0	25.3±0.1	45.3±0.0	14.2±0.0	35.8±0.2	57.6±0.1
CFA (Ours)	fa	✓	8.4±0.0	24.6±0.1	43.9±0.0	14.2±0.1	36.3±0.2	56.1±0.0

Table 2: Method comparison on each adaptation tasks. The evaluation metric is top-1 error rate. The results of CIFAR-10-C, CIFAR-100-C and ImageNet-C are ones averaged over the 15 corruption types with highest severity level (=5). CFA-F : Overall distribution matching only. CFA-C : Class-conditional distribution matching only. gf : Gradient free method. fm : Method that controls the output feature representation (without depending on feature alignment) by modulation. fa : Method that utilizes feature alignment between source and target by modulation. Our proposal (CFA-C and CFA) is the only method utilizing the class-conditional feature alignment during test-time adaptation.

4 Experiment

4.1 Datasets and Task Design

Common Corruptions. We validate the robustness against common corruptions on CIFAR-10-C, CIFAR-100-C and ImageNet-C [Hendrycks and Dietterich, 2019] as target datasets. These datasets contain data with 15 types corruptions with five levels of severity, that is, each dataset has 75 distinct corruptions. Most of our experiments use the highest severity(=5) datasets as they can make the difference in performance most noticeable. As source datasets, CIFAR-10, CIFAR-100 [Krizhevsky and Hinton, 2009] and ImageNet(-2012) [Russakovsky *et al.*, 2015] are used, respectively.

Domain Adaptation. We validate the robustness against style shift on small-sized datasets and large-sized datasets. For small-sized datasets, we evaluate the adaptation from SVHN to MNIST / MNIST-M [Netzer *et al.*, 2011; Lecun *et al.*, 1998; Ganin and Lempitsky, 2015]. For large-sized datasets, we evaluate the adaptation from ImageNet to ImageNet-Sketch [Wang *et al.*, 2019]. See Appendix A for a detail description of each dataset.

4.2 Implementation Details

Vision Transformer (ViT-B16) is used as a default model throughout the experiment unless an explicit explanation is provided. Images of all the datasets are resized to 224×224 (see Appendix B for details). Before adaptation, the model is fine-tuned on each source dataset (see Appendix C for details). In addition, the central moments statistics of hidden representation based on source data need to be calculated to store them in memory. For this purpose, we use all the training data in the source dataset and set the dropout [Srivastava *et al.*, 2014] off in the model during the calculation.

As for default hyperparameters for adaptation on target data, batch size is set as 64, optimizer is set as SGD with a constant learning rate of 0.001, and momentum of 0.9 with gradient clipping [Zhang *et al.*, 2020] at global norm 1.0 across all the experiments (Gradient clipping has the effect

of preventing adaptation by Tent from catastrophic failure in the severe corruption setting. See ‘‘Ablation Study’’ in §4.4). As for CFA, the balancing parameter λ is set as 1.0, and maximum central moments order K is set as 3. During prediction and parameter update, dropout is set off in models.

As an evaluation metric, top-1 error of classification is used across all the experiments. We run all the experiments three times with different seeds for different data ordering by shuffling. A mean and unbiased standard deviation of the metric are reported. Our implementation is in PyTorch [Paszke *et al.*, 2019]. We use various backbone networks from timm library [Wightman, 2019] and torchvision library (Appendix D). Every experiment is run on cloud A100 x 1GPU instance.

4.3 Baseline Methods

We compare CFA with some existing baseline test-time adaptation methods that do not need to alter training phase as described in §2.2: **Tent**, **PL**, **TFA(-)**³, **T3A** and **SHOT-IM**. In addition, we report the performance of the model on target datasets without any adaptation as **Source**. T-BN is excluded from the baseline because some models (ViT variants and MLP-Mixer) do not have a batch normalization layer. For a fair comparison, we use the same hyperparameters across all the methods as described in §4.2.

4.4 Experiment Result

Modulation Study. Table 1 answers the question about which set of modulation parameters is the most suitable for improving the performance of test-time adaptations on ViTs. There are two findings. First, updating layer normalization parameters can achieve balanced and high performance across all the main methods. Second, SHOT-IM and CFA achieve

³Original TFA needs to alter training phase (add contrastive learning), while this study focuses on robustifying large-scale models without retraining them from scratch. Therefore, we have changed some of the settings from the original TFA so that the model does not need to alter training phase. The modified version of TFA is denoted as TFA(-) in our experiments. See Appendix F for details.

	ImageNet-C	ImageNet-S
ResNet50	82.0±0.0	75.4±0.0
+ CFA / SHOT-IM	58.8±0.0/58.8±0.0	70.0±0.2/ 69.2±0.1
ResNet101	77.4±0.0	72.3±0.0
+ CFA / SHOT-IM	55.3±0.1/55.7±0.0	66.8±0.0/ 66.2±0.1
ViT-B16	61.9±0.0	64.1±0.0
+ CFA / SHOT-IM	43.9±0.0/45.7±0.0	56.0±0.1/56.1±0.1
ViT-L16	53.4±0.0	59.1±0.0
+ CFA / SHOT-IM	40.2±0.0/42.0±0.0	52.6±0.0/53.6±0.1
DeiT-S16	59.9±0.0	66.6±0.0
+ CFA / SHOT-IM	46.0±0.0/46.1±0.0	60.3±0.1/ 59.4±0.0
DeiT-B16	52.9±0.0	62.5±0.0
+ CFA / SHOT-IM	39.9±0.0/39.9±0.0	55.9±0.0/ 55.4±0.0
MLP-Mixer-B16	73.3±0.0	74.3±0.0
+ CFA / SHOT-IM	52.4±0.1/55.1±0.1	64.2±0.1/65.9±0.2
MLP-Mixer-L16	77.1±0.0	79.8±0.0
+ CFA / SHOT-IM	56.3±0.0/62.4±0.1	70.8±0.3/72.9±0.3
ViT-B16-AugReg	49.0±0.0	57.0±0.0
+ CFA / SHOT-IM	37.6±0.0/38.4±0.0	51.5±0.1/ 51.0±0.2
ViT-L16-AugReg	39.1±0.0	48.2±0.0
+ CFA / SHOT-IM	32.1±0.0/33.3±0.0	45.2±0.0/45.6±0.1
BeiT-B16	48.3±0.0	52.6±0.0
+ CFA / SHOT-IM	35.4±0.0/37.6±0.0	47.5±0.0/49.1±0.0
BeiT-L16	35.9±0.0	44.2±0.0
+ CFA / SHOT-IM	26.0±0.0/28.2±0.0	39.9±0.1/41.5±0.0

Table 3: Adaptation results based on several backbone networks. The evaluation metric of ImageNet-C is the averaged top-1 error over 15 corruption types with a severity level of 5. We use publicly available models that were already fine-tuned on ImageNet.

higher performance by updating all or feature extractor parameters, while Tent and PL deteriorates the performance because of catastrophic failure (See Appendix I for details). This indicates that a method with more sophisticated strategy within the adaptation function can work properly without sensibly selecting modulation parameters. In all the subsequent experiments, we choose layer normalization as modulation parameters across all the methods for the fair comparison.

CFA Outperforms Existing Methods on Several Datasets.

Table 2 summarizes the adaptation result across datasets for each test time adaptation methods. As for CIFAR-10-C, CIFAR-100-C, and ImageNet-C, we measure the averaged top-1 error across 15 corruption types for the highest severity level (=5). CFA (our method) aligns both the overall distribution and class-conditional distribution between source and target datasets. In addition to CFA, we have experimented class-conditional distribution matching only method (CFA-C) and overall distribution matching only method (CFA-F) to measure the contribution of each distribution matching to performance. Specifically, the objective function of CFA-C and CFA-F is respectively defined as Eq.(10) and Eq.(9). The experiment results demonstrate that CFA can achieve the best or comparable performance against baseline methods across all datasets. It is also verified that CFA-F and CFA-C can

Severity	Source	Tent	SHOT-IM	CFA
1	16.8±0.0	15.4±0.0	15.8±0.0	15.3±0.0
2	20.3±0.0	17.9±0.0	18.4±0.0	17.5±0.0
3	22.5±0.0	19.6±0.4	19.9±0.0	18.7±0.0
4	27.2±0.0	24.0±1.2	23.2±0.0	21.5±0.0
5	35.9±0.0	33.6±0.1	28.2±0.0	26.0±0.0
Average	24.5±0.0	22.1±0.3	21.1±0.0	19.8±0.0

Table 4: Top-1 error rate on ImageNet-C averaged across all the severity level and 15 corruption types. BeiT-L16 is used as a model.

Method	W/. Eq(1)(5)	W/O. Eq(1)(5)
Source	61.95±0.00	61.95±0.00
CFA-F ($K=1$)	46.69±0.02	46.69±0.01
CFA-F ($K=3$)	46.66±0.02	47.28±0.03
CFA-F ($K=5$)	46.64±0.02	54.51±0.14
CFA-C	45.31±0.03	47.13±0.06
CFA ($K=1$)	43.98±0.04	45.28±0.02
CFA ($K=3$)	43.90±0.04	44.56±0.03
CFA ($K=5$)	43.90±0.04	52.25±0.11

Table 5: Ablation study of CFA. Top-1 error on ImageNet-C averaged over 15 corruption types with severity level of 5. ViT-B16 is used. CFA-F : Overall distribution matching only. CFA-C : Class-conditional distribution matching only. K : Maximum # of central moments. K=1 denotes first-order moment (mean) matching only.

solely achieve better performance compared to the case without adaptation (“Source”) as in Table 2. Finally, CFA further boosts the performance on most datasets by combining them.

CFA Is Model Agnostic. Table 3 shows the adaptation results on ImageNet-C and ImageNet-Sketch by CFA (and SHOT-IM for comparison) based on various category’s backbone networks. Specifically, we used publicly available models that are already fine-tuned on ImageNet-2012 at a resolution of 224×224 , including ResNet, ViT, ViT-AugReg, DeiT, BeiT, and MLP-Mixer. See Appendix D for details. The modulation parameters are BN for ResNet, and LN for the others. The results indicate that our method (CFA) consistently improves the performance regardless of the backbone networks. It is also found that the better performance on the source dataset (ImageNet), the stronger robustness on the target dataset (ImageNet-C) the model can gain by adaptation. See Appendix E for visualization of the relationship.

CFA Achieves SOTA Performance. Among these backbone networks, we select BeiT-L16, which achieved strong performance on ImageNet, and calculate the top-1 error rate on ImageNet-C averaged over 15 types of corruptions and all the severity levels (1-5) for each TTA methods. The results described in Table 4 demonstrate that 19.8% using CFA on BeiT-L16 gives superior performance to the other baseline methods. It also outperforms the existing test-time adaptation result 44.0% using Tent on ResNet50 [Wang *et al.*, 2020]. Therefore, CFA achieves the state-of-the-art (SOTA) performance among TTA methods that do not need to alter training phase (See Appendix I for the full results).

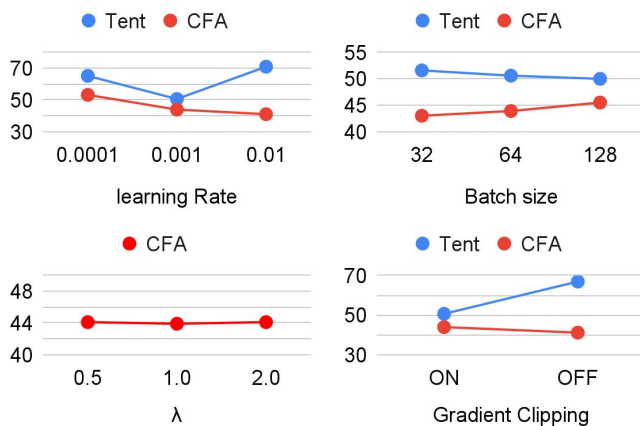


Figure 1: The effect of changing hyperparameters on Tent and CFA performance. The evaluation metric is the top-1 error on ImageNet-C averaged over 15 corruption types with a severity level of 5. ViT-B16 is used as a model. Either one of the hyperparameter values is changed from the default described in §4.2.

Ablation Study. Table 5 summarizes the ablation study results to analyze the detailed contributions of each components in our method on the robustness. Specifically, we analyze the effect of the normalization of hidden representation before calculating the distribution statistics by comparing the scenarios of with/without Eq.(1) and (5). In the case of CFA-F, it is verified that the performance deteriorates significantly without Eq.(1) and (5) especially when the maximum number of moments K gets larger. This indicates that feature normalization, especially bounding minimum and maximum value of hidden representation, stabilizes the performance of matching higher order moments. In the case of CFA-C, it is verified that the performance deteriorates without Eq.(1) and (5). It is speculated that feature normalization, especially layer normalization without affine transformation, might have a positive effect on class-conditional (centroid) distribution matching by highlighting the distribution property for each class. In addition, it is also verified that using both overall feature alignment and class-conditional feature alignment (CFA) boosts the performance compared to either alone (CFA-F or CFA-C) regardless of the value of K .

Hyperparameter Sensitivity. For online adaptation, hyperparameter selection is a challenging issue. Figure 1 shows the experiment results about each hyperparameter sensitivity on ImageNet-C with the highest severity level ($=5$) averaged over 15 corruption types. We checked 4 hyperparameters by changing either one of the values from the default described in §4.2. (a) learning rate, (b) batch size, (c) balancing hyperparameter λ , and (d) whether to enable gradient clipping for SGD optimization. The finding is that Tent is more sensitive to some hyperparameters than CFA. In particular, enabling gradient clipping is essential when applying Tent to ViT to avoid catastrophic failure, while it is not essential for CFA. Furthermore, large learning rate also causes Tent catastrophic failure. In contrast, CFA is robust to all the above hyperparameters. This indicates that we can safely use CFA in unknown environments with rough hyperparameter selection.

5 Conclusion

This is the first study that verifies the effectiveness of test-time adaptation methods on ViT to boost their robustness. Experiment results demonstrate that the existing methods can be applied to ViT and the prior-convention (sensibly selecting modulation parameters) is not necessary when a proper loss function is used. This study also proposed a novel method, CFA, which is hyperparameter friendly, model agnostic, and surpasses existing baselines. We hope this study becomes a milestone of TTA for current large models and will serve as a stepping stone to TTA for larger models in the future.

Acknowledgements

This work has been supported by the Mohammed bin Salman Center for Future Science and Technology for Saudi-Japan Vision 2030 at The University of Tokyo (MbSC2030). Computational resource of AI Bridging Cloud Infrastructure (ABCI) provided by National Institute of Advanced Industrial Science and Technology (AIST) was used for experiments.

References

- [Ba *et al.*, 2016] Jimmy Lei Ba, Jamie Ryan Kiros, and Geoffrey E Hinton. Layer normalization. *arXiv preprint arXiv:1607.06450*, 2016.
- [Bao *et al.*, 2021] Hangbo Bao, Li Dong, and Furu Wei. Beit: Bert pre-training of image transformers. *arXiv preprint arXiv:2106.08254*, 2021.
- [Bhojanapalli *et al.*, 2021] Srinadh Bhojanapalli, Ayan Chakrabarti, Daniel Glasner, Daliang Li, Thomas Unterthiner, and Andreas Veit. Understanding robustness of transformers for image classification. In *Proceedings of the IEEE/CVF ICCV*, pages 10231–10241, 2021.
- [Carion *et al.*, 2020] Nicolas Carion, Francisco Massa, Gabriel Synnaeve, Nicolas Usunier, Alexander Kirillov, and Sergey Zagoruyko. End-to-end object detection with transformers. In *ECCV*, pages 213–229. Springer, 2020.
- [Chen *et al.*, 2022] Xiangning Chen, Cho-Jui Hsieh, and Boqing Gong. When vision transformers outperform resnets without pre-training or strong data augmentations. In *ICLR*, 2022.
- [Deng *et al.*, 2009] Jia Deng, Wei Dong, Richard Socher, Li-Jia Li, Kai Li, and Li Fei-Fei. Imagenet: A large-scale hierarchical image database. In *CVPR*, pages 248–255, 2009.
- [Deng *et al.*, 2019] Zhijie Deng, Yucen Luo, and Jun Zhu. Cluster alignment with a teacher for unsupervised domain adaptation. In *Proceedings of ICCV*, pages 9944–9953, 2019.
- [Dosovitskiy *et al.*, 2020] Alexey Dosovitskiy, Lucas Beyer, Alexander Kolesnikov, Dirk Weissenborn, Xiaohua Zhai, Thomas Unterthiner, Mostafa Dehghani, Matthias Minderer, Georg Heigold, Sylvain Gelly, et al. An image is worth 16x16 words: Transformers for image recognition at scale. In *ICLR*, 2020.
- [Ganin and Lempitsky, 2015] Yaroslav Ganin and Victor Lempitsky. Unsupervised domain adaptation by backpropagation. In *ICML*, pages 1180–1189. PMLR, 2015.
- [Hendrycks and Dietterich, 2019] Dan Hendrycks and Thomas Dietterich. Benchmarking neural network robustness to common corruptions and perturbations. *Proc. of the ICLR*, 2019.
- [Hendrycks *et al.*, 2019] Dan Hendrycks, Norman Mu, Ekin D Cubuk, Barret Zoph, Justin Gilmer, and Balaji Lakshminarayanan. Augmix: A simple data processing method to improve robustness and uncertainty. *arXiv preprint arXiv:1912.02781*, 2019.

- [Hendrycks *et al.*, 2020] Dan Hendrycks, Steven Basart, Norman Mu, Saurav Kadavath, Frank Wang, Evan Dorundo, Rahul Desai, Tyler Zhu, Samyak Parajuli, Mike Guo, et al. The many faces of robustness: A critical analysis of out-of-distribution generalization. *arXiv preprint arXiv:2006.16241*, 2020.
- [Ioffe and Szegedy, 2015] Sergey Ioffe and Christian Szegedy. Batch normalization: Accelerating deep network training by reducing internal covariate shift. In *ICML*, pages 448–456. PMLR, 2015.
- [Iwasawa and Matsuo, 2021] Yusuke Iwasawa and Yutaka Matsuo. Test-time classifier adjustment module for model-agnostic domain generalization. In *Advances in NeurIPS*, 2021.
- [Krizhevsky and Hinton, 2009] Alex Krizhevsky and Geoffrey Hinton. Learning multiple layers of features from tiny images. Technical report, University of Toronto, 2009.
- [LeCun *et al.*, 1998] Yann LeCun, Léon Bottou, Yoshua Bengio, and Patrick Haffner. Gradient-based learning applied to document recognition. *Proceedings of the IEEE*, 86(11):2278–2324, 1998.
- [Lee and others, 2013] Dong-Hyun Lee et al. Pseudo-label: The simple and efficient semi-supervised learning method for deep neural networks. In *Workshop on challenges in representation learning, ICML*, volume 3, page 896, 2013.
- [Lester *et al.*, 2021] Brian Lester, Rami Al-Rfou, and Noah Constant. The power of scale for parameter-efficient prompt tuning. In *Proceedings of EMNLP*, pages 3045–3059, 2021.
- [Liang *et al.*, 2020] Jian Liang, Dapeng Hu, and Jiashi Feng. Do we really need to access the source data? source hypothesis transfer for unsupervised domain adaptation. In *ICML*, pages 6028–6039. PMLR, 2020.
- [Liu *et al.*, 2021] Yuejiang Liu, Parth Kothari, Bastien Geman van Delft, Baptiste Bellot-Gurlet, Taylor Mordan, and Alexandre Alahi. TTT++: When does self-supervised test-time training fail or thrive? In *Advances in NeurIPS*, 2021.
- [Morrison *et al.*, 2021] Katelyn Morrison, Benjamin Gilby, Colton Lipchak, Adam Mattioli, and Adriana Kovashka. Exploring corruption robustness: Inductive biases in vision transformers and mlp-mixers. *arXiv preprint arXiv:2106.13122*, 2021.
- [Nado *et al.*, 2020] Zachary Nado, Shreyas Padhy, D Sculley, Alexander D’Amour, Balaji Lakshminarayanan, and Jasper Snoek. Evaluating prediction-time batch normalization for robustness under covariate shift. *arXiv preprint arXiv:2006.10963*, 2020.
- [Naseer *et al.*, 2021] Muzammal Naseer, Kanchana Ranasinghe, Salman Khan, Munawar Hayat, Fahad Shahbaz Khan, and Ming-Hsuan Yang. Intriguing properties of vision transformers. *arXiv preprint arXiv:2105.10497*, 2021.
- [Netzer *et al.*, 2011] Yuval Netzer, Tao Wang, Adam Coates, Alessandro Bissacco, Bo Wu, and Andrew Y. Ng. Reading digits in natural images with unsupervised feature learning. In *NIPS Workshop*, 2011.
- [Paszke *et al.*, 2019] Adam Paszke, Sam Gross, Francisco Massa, Adam Lerer, James Bradbury, Gregory Chanan, Trevor Killeen, Zeming Lin, Natalia Gimelshein, Luca Antiga, et al. Pytorch: An imperative style, high-performance deep learning library. *Advances in NeurIPS*, pages 8026–8037, 2019.
- [Paul and Chen, 2021] Sayak Paul and Pin-Yu Chen. Vision transformers are robust learners. *arXiv preprint arXiv:2105.07581*, 2(3), 2021.
- [Rusak *et al.*, 2020] Evgenia Rusak, Lukas Schott, Roland S Zimmermann, Julian Bitterwolf, Oliver Bringmann, Matthias Bethge, and Wieland Brendel. A simple way to make neural networks robust against diverse image corruptions. In *ECCV*, pages 53–69. Springer, 2020.
- [Russakovsky *et al.*, 2015] Olga Russakovsky, Jia Deng, Hao Su, Jonathan Krause, Sanjeev Satheesh, Sean Ma, Zhiheng Huang, Andrej Karpathy, Aditya Khosla, Michael Bernstein, et al. Imagenet large scale visual recognition challenge. *IJCV*, 115(3):211–252, 2015.
- [Schneider *et al.*, 2020] Steffen Schneider, Evgenia Rusak, Luisa Eck, Oliver Bringmann, Wieland Brendel, and Matthias Bethge. Improving robustness against common corruptions by covariate shift adaptation. *Advances in NeurIPS*, 33, 2020.
- [Srivastava *et al.*, 2014] Nitish Srivastava, Geoffrey Hinton, Alex Krizhevsky, Ilya Sutskever, and Ruslan Salakhutdinov. Dropout: a simple way to prevent neural networks from overfitting. *The JMLR*, 15(1):1929–1958, 2014.
- [Steiner *et al.*, 2021] Andreas Steiner, Alexander Kolesnikov, Xiaohua Zhai, Ross Wightman, Jakob Uszkoreit, and Lucas Beyer. How to train your vit? data, augmentation, and regularization in vision transformers. *arXiv preprint arXiv:2106.10270*, 2021.
- [Tolstikhin *et al.*, 2021] Ilya Tolstikhin, Neil Houlsby, Alexander Kolesnikov, Lucas Beyer, Xiaohua Zhai, Thomas Unterthiner, Jessica Yung, Daniel Keysers, Jakob Uszkoreit, Mario Lucic, et al. Mlp-mixer: An all-mlp architecture for vision. *arXiv preprint arXiv:2105.01601*, 2021.
- [Touvron *et al.*, 2021] Hugo Touvron, Matthieu Cord, Matthijs Douze, Francisco Massa, Alexandre Sablayrolles, and Hervé Jégou. Training data-efficient image transformers & distillation through attention. In *ICML*, pages 10347–10357, 2021.
- [Vaswani *et al.*, 2017] Ashish Vaswani, Noam Shazeer, Niki Parmar, Jakob Uszkoreit, Llion Jones, Aidan N Gomez, Łukasz Kaiser, and Illia Polosukhin. Attention is all you need. In *Advances in NeurIPS*, pages 5998–6008, 2017.
- [Wang *et al.*, 2019] Haohan Wang, Songwei Ge, Zachary Lipton, and Eric P Xing. Learning robust global representations by penalizing local predictive power. In *Advances in NeurIPS*, pages 10506–10518, 2019.
- [Wang *et al.*, 2020] Dequan Wang, Evan Shelhamer, Shaoteng Liu, Bruno Olshausen, and Trevor Darrell. Tent: Fully test-time adaptation by entropy minimization. In *ICLR*, 2020.
- [Wightman, 2019] Ross Wightman. Pytorch image models. <https://github.com/rwightman/pytorch-image-models>, 2019. Accessed: 2021-12-27.
- [Xie *et al.*, 2018] Shaoan Xie, Zibin Zheng, Liang Chen, and Chuan Chen. Learning semantic representations for unsupervised domain adaptation. In *ICML*, pages 5423–5432, 2018.
- [Yamada and Otani, 2022] Yutaro Yamada and Mayu Otani. Does robustness on imagenet transfer to downstream tasks? In *Proceedings of the IEEE/CVF Conference CVPR*, pages 9215–9224, June 2022.
- [Zellinger *et al.*, 2017] Werner Zellinger, Thomas Grubinger, Edwin Lughofer, Thomas Natschläger, and Susanne Saminger-Platz. Central moment discrepancy (CMD) for domain-invariant representation learning. In *5th ICLR*, 2017.
- [Zeng *et al.*, 2020] Yanhong Zeng, Jianlong Fu, and Hongyang Chao. Learning joint spatial-temporal transformations for video inpainting. In *ECCV*, pages 528–543. Springer, 2020.
- [Zhang *et al.*, 2020] Jingzhao Zhang, Tianxing He, Suvrit Sra, and Ali Jadbabaie. Why gradient clipping accelerates training: A theoretical justification for adaptivity. In *ICLR*, 2020.
- [Zhou *et al.*, 2018] Luwei Zhou, Yingbo Zhou, Jason J Corso, Richard Socher, and Caiming Xiong. End-to-end dense video captioning with masked transformer. In *Proceedings of the IEEE Conference on CVPR*, pages 8739–8748, 2018.

A Datasets Description

A.1 CIFAR-10/100 and ImageNet

CIFAR-10 / CIFAR-100 and ImageNet are used as source datasets for our experiments. CIFAR-10 / CIFAR-100 are respectively 10-class / 100-class color image datasets including 50,000 training data and 10,000 test data with a resolution of 32×32 . ImageNet is a 1000-class image dataset with more than 1.2 million training data and 50,000 validation data with various resolutions.

A.2 Corruption Datasets

CIFAR-10-C / CIFAR-100-C and ImageNet-C [Hendrycks and Dietterich, 2019] are used as target datasets for our experiment. These datasets contain data with 15 types of corruptions with five levels of severity. Therefore, each dataset has 75 varieties of corruptions in total. Each corrupted data is composed of data from original CIFAR-10 and CIFAR-100 test images, and ImageNet validation images. Therefore, the CIFAR-10-C/CIFAR-100-C consists of 10,000 images for each corruption/type and ImageNet-C dataset consists of 50,000 images for each corruption/type. Fig.2 illustrates examples of 15 corruption types from ImageNet-C. These examples are cited from [Hendrycks and Dietterich, 2019]. CIFAR-10-C and CIFAR-100-C have the same corruption types. Figure.3 illustrates examples for each corruption severity levels from 1 to 8 of Gaussian Noise. ImageNet-C dataset contains only images of severity level from 1 to 5. We have augmented the severity levels of Gaussian Noise datasets from 6 to 8 following the same setting as [Rusak *et al.*, 2020] to use them for the corruption severity experiment on Table.7.

A.3 Digits Datasets

SVHN, MNIST and MNIST-M are 10-class classification datasets for digit recognition ranging from 0 to 9. SVHN[Netzer *et al.*, 2011] is used as source dataset. The total number of training data is 73,257. Test data of MNIST[LeCun *et al.*, 1998] and MNIST-M[Ganin and Lempitsky, 2015] are used as target. The total numbers of test dataset used for adaptation are 10,000 and 10,000, respectively. MNIST data is a gray scale image, so we convert the image into an RGB scale as a data preprocessing. Figure.4 illustrates some image examples from SVHN, MNIST and MNIST-M.

A.4 ImageNet-Sketch

ImageNet-Sketch [Wang *et al.*, 2019] is used as target datasets for our experiments. ImageNet-Sketch contains 50,000 sketch images, 50 images for each of the 1,000 ImageNet classes. Figure.5 illustrates image examples from ImageNet-Sketch. Most images are mono-color, but RGB resolution.

B Dataset Pre-processing

For this experiment, images of all datasets are resized to 224×224 . For ImageNet, some images are rectangular, so all the images are resized with fixed aspect ratio so that

the shorter side of the rectangle is 256, followed by center-cropping with a size of 224×224 . ImageNet-C data have already been pre-processed in the same way and are publicly available. ImageNet-Sketch samples are resized to 224 in the same way and center-cropped with a size of 224×224 . When using ViT-B16, which is a baseline model for our experiment, pixels of images are rescaled from $[0, 255]$ to $[-1, 1]$ by taking the mean and std as $[0.5, 0.5, 0.5]$ and $[0.5, 0.5, 0.5]$ across all the datasets. See Table.9 for the other models.

C Fine-Tuning Details

Vision Transformer(ViT) is used as a basic model for this experiment. Before adaptation, the model needs to be fine-tuned for each dataset. For CIFAR-10, CIFAR-100 and SVHN, we use ViT-B16 parameters that is already pre-trained on ImageNet-21K[Deng *et al.*, 2009], which is a large dataset with 21k classes and 14M images. For fine-tuning hyperparameters, following [Dosovitskiy *et al.*, 2020], We use batch size of 512, set optimizer as SGD with momentum 0.9 and gradient clipping at global norm 1.0. We choose a learning rate of 0.03. We apply a cosine schedule of 500 warmup steps and the total number of iterations as 2000 for CIFAR-100 and SVHN. We apply cosine schedule of 200 warmup steps and the total number of iteration as 1000 for CIFAR-10. The fine-tuning result is 1.1% Top-1 error for CIFAR-10, 6.8% for CIFAR-100, and 3.0% for SVHN. For ImageNet, we use publicly available ViT-B16 parameters that are already pre-trained for ImageNet-21K and fine-tuned for ImageNet(-2012). Therefore, fine-tuning on ImageNet is not required. The Top-1 error for ImageNet is 18.6% in our setting.

D Detailed information about the backbone networks used in Table 3

Table.8 summarizes the detailed information about the backbone networks. Note that all the models used are already pre-trained on ImageNet-2012 at resolution 224×224 and publicly available. For model agnostic study, pixels are rescaled by taking the mean and std as described at Table 9.

E Visualization of Model Agnosticity Study

Figure 6 visualizes the relationship between the Top-1 error rate on ImageNet (Source dataset) and the Top-1 error rate on ImageNet-C (Target dataset) before / after the CFA adaptation for each backbone network.

F Detail Settings of Baseline Methods

F.1 TFA(-)

Test-time feature alignment (TFA) [Liu *et al.*, 2021] aligns the hidden representation on target data by minimizing the distance of the mean vector $\mu^s, \mu^t \in \mathbb{R}^D$ and covariance matrix $\Sigma^s, \Sigma^t \in \mathbb{R}^{D \times D}$ between source and target. D is the dimension size of the hidden representation. We focus only on the "Online Feature Alignment" part in TTT++ [Liu *et al.*, 2021]. Original TFA [Liu *et al.*, 2021] aligns the distributions at both the hidden representation and the output of the self-supervised head. However, in our experiment, TFA(-) does

not employ self-supervised learning, so we only focus on distribution matching of the hidden representation. Specifically, in this experiment, the hidden representation to align is defined as the one before the classifier head $h(x) = f(x; \phi)$. The loss function is $\mathcal{L} = \beta_1 \|\mu^s - \mu^t\|_2^2 + \beta_2 \|\Sigma^s - \Sigma^t\|_F^2$ where $\|\cdot\|_2$ is the Euclidean norm and $\|\cdot\|_F$ is the Frobenius norm. β_1 and β_2 are balancing hyperparameters. Like CFA, TFA(-) calculates the statistics on source dataset and store them in memory before adaptation. Note that "Online Dynamic Queue" [Liu *et al.*, 2021] is not used in TFA(-) in our experiment. Table 6 describes the small experiment results of TFA(-) on ImageNet-C datasets with severity=5 by changing the balancing hyperparameters β_1, β_2 . Following [Liu *et al.*, 2021], we use $\beta_1 = 1, \beta_2 = 1$ for the main experiment in Table 2.

Method	ImageNet-C
TFA(-) ($\beta_1 = 1, \beta_2 = 1$)	57.7±0.1
TFA(-) ($\beta_1 = 1, \beta_2 = 1/D$)	48.8±0.0
TFA(-) ($\beta_1 = 1, \beta_2 = 0$)	46.7±0.0
TFA(-) ($\beta_1 = 0, \beta_2 = 1/D$)	65.5±0.4
TFA(-) ($\beta_1 = 1/D, \beta_2 = 1/D$)	61.0±0.1
TFA(-) ($\beta_1 = 1/D, \beta_2 = 1/D^2$)	51.8±0.0
TFA(-) ($\beta_1 = 1/D, \beta_2 = 0$)	51.8±0.0
TFA(-) ($\beta_1 = 0, \beta_2 = 1/D^2$)	62.0±0.0

Table 6: Experiment results of TFA(-) on ImageNet-C by changing the balancing hyperparameters β_1, β_2 . Evaluation metric is Top-1 error on ImageNet-C averaged over 15 corruption types with severity level=5. ViT-B16 is used as a model.

F.2 T3A

T3A [Iwasawa and Matsuo, 2021] updates the centroid of each class averaging over the pseudo labeled samples' feature vectors in an online manner. This is a gradient-free approach and there is no loss function. The hyperparameter filter size K is set to 100 in our experiment.

G Central Moment Distance (CMD)

Our proposal utilizes central moment distance (CMD) [Zellinger *et al.*, 2017] as to minimize the overall distribution differences between the source and target data. CMD is an existing approach for UDA settings. Formally, let X and Y be bounded random samples with respective probability distributions p and q on the interval $[a; b]^N$. CMD is defined by

$$\begin{aligned}
 CMD_k &= \frac{1}{|b-a|} \|\mathbb{E}(X) - \mathbb{E}(Y)\|_2 \\
 &+ \frac{1}{|b-a|^k} \sum_{k=2}^K \|\mathbb{M}_k(X) - \mathbb{M}_k(Y)\|_2,
 \end{aligned} \tag{12}$$

where $\mathbb{E}(X) = \frac{1}{|X|} \sum_x$ is the empirical expectation vector computed for the sample X , and $\mathbb{M}_k(X) = \mathbb{E}((x - \mathbb{E}(X))^k)$ is the vector of all k^{th} order central moments of the coordinates of X . Y follows the same idea. Previous studies

Severity (std)	Source	Tent w/o GC	Tent w/ GC	CFA w/ GC
1 (0.08)	23.3±0.0	22.0±0.1	22.0±0.0	22.1±0.1
2 (0.12)	26.9±0.0	24.8±0.0	24.9±0.1	25.0±0.0
3 (0.18)	35.6±0.0	30.5±0.1	31.1±0.1	30.6±0.1
4 (0.26)	52.0±0.0	59.8±23.0	41.6±0.1	40.0±0.0
5 (0.38)	77.7±0.0	97.3±0.3	66.3±8.8	56.5±0.1
6 (0.50)	92.7±0.0	99.8±0.1	99.1±0.3	72.0±0.1
7 (0.60)	97.4±0.0	99.9±0.0	99.8±0.0	82.4±0.1
8 (0.70)	99.0±0.0	99.9±0.0	99.9±0.0	89.8±0.2

Table 7: Top-1 error based on Gaussian Noise Dataset for each severity. ViT-B16 is used as a model. GC : Gradient Clipping. σ : Standard deviation of Gaussian noise. We additionally create severity level 6-8 by adding the noise to the ImageNet validation data.

have focused on using CMD in the field of UDA to reduce the distributional gaps between source and target representations. However, CMD can also be potentially used for test-time adaptation because it does not need to store the source dataset itself; instead, we store central moment statistics of the source data in memory, and use it during online adaptation for moment matching between source and target.

H Further Study on Severe Corruption

We further analyse the robustness of Tent and CFA from the severity viewpoint. The detail experiment setting is the same as described at §4.2. Table 7 summarizes the results on Gaussian Noise for each severity level from 1 to 8. Original ImageNet-C contains only severity level of until 5, so we create the severe corrupted images (severity 6, 7 and 8) specific to Gaussian Noise by increasing the standard deviation. We found that gradient clipping [Zhang *et al.*, 2020] is essential to use Tent in ViT, which are not used in the original study. Specifically, we clip the global norm of gradients to 1.0. Without gradient clipping, Tent often gave catastrophic failure. However, even with gradient clipping, when the noise is severer, Tent causes catastrophic failure while CFA avoids it during adaptation.

I Detail Experiment Results

I.1 Detail Results for Table.1

See Table.10 and 11.

I.2 Detail Results for Table.2

See Table.12.

I.3 Detail Results for Table.3

See Table.13, 14 and 15.

I.4 Detail Results for Table.4

See Table.16.

I.5 Detail Results for Table.5

See Table.18.

I.6 Detail Results for Figure.1

See Table.17.

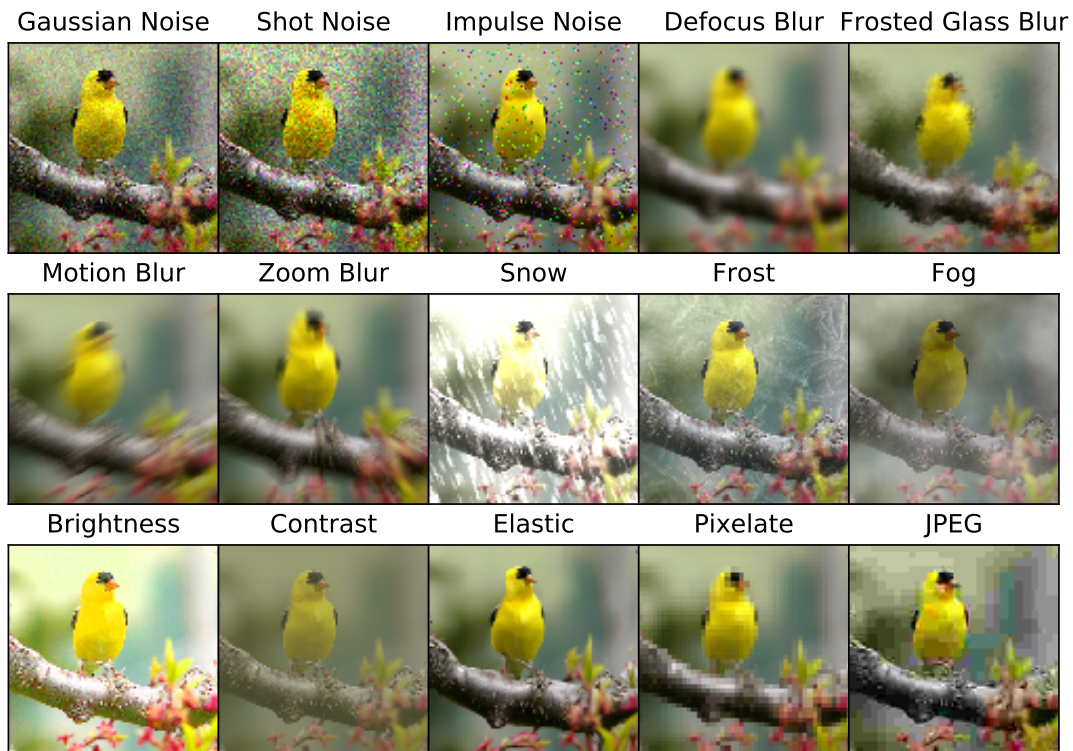


Figure 2: Examples of 15 corruption types from ImageNet-C. These images are borrowed from [Hendrycks and Dietterich, 2019]. CIFAR-10-C and CIFAR-100-C have the same corruption types.

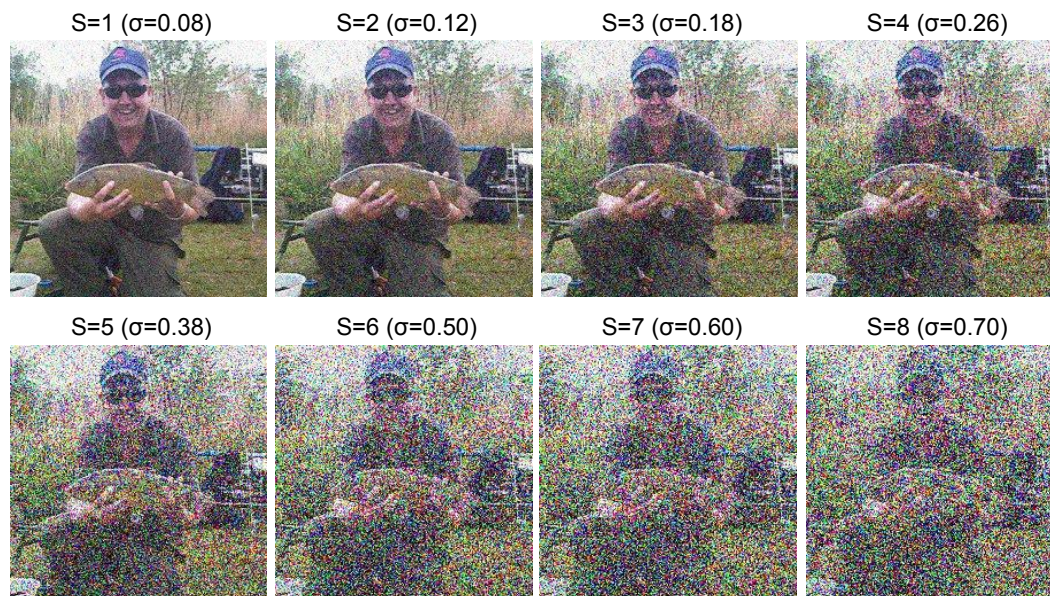


Figure 3: Example images of different severity levels. S : Severity Level. σ : standard deviation of Gaussian Noise. Images with severity level 1-5 are from ImageNet-C. Images with severity level 6-8 are created by adding Gaussian noise to the original ImageNet validation dataset.



Figure 4: Examples from Digit recognition Datasets.

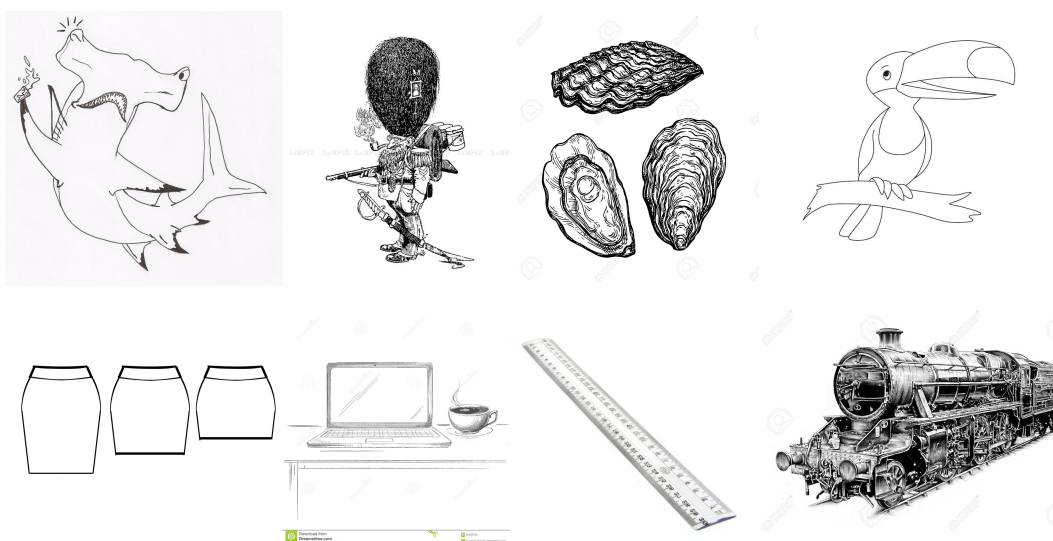


Figure 5: Examples from ImageNet-Sketch Dataset.

Backbone Networks	Pytorch Library(Ver.)	Model Name in Library	ImageNet Top-1 Error Rate
ResNet50	torchvision(0.10.0)	resnet50	24.8
ResNet101	torchvision(0.10.0)	resnet101	23.4
ViT-B16	timm(0.4.9)	vit_base_patch16_224	18.6
ViT-L16	timm(0.4.9)	vit_large_patch16_224	17.1
DeiT-S16	timm(0.5.0)	deit_small_distilled_patch16_224	19.0
DeiT-B16	timm(0.5.0)	deit_base_distilled_patch16_224	16.8
MLP-Mixer-B16	timm(0.5.0)	mixer_b16_224	23.5
MLP-Mixer-L16	timm(0.5.0)	mixer_l16_224	28.2
ViT-B16 (AugReg)	timm(0.5.0)	vit_base_patch16_224	15.6
ViT-L16 (AugReg)	timm(0.5.0)	vit_base_patch16_224	14.3
BeiT-B16	timm(0.5.0)	beit_base_patch16_224	15.0
BeiT-L16	timm(0.5.0)	beit_large_patch16_224	12.7

Table 8: Backbone networks information used in Table 3

Backbone Network	MEAN	STD
ResNet50	[0.485, 0.456, 0.406]	[0.229, 0.224, 0.225]
ResNet101	[0.485, 0.456, 0.406]	[0.229, 0.224, 0.225]
ViT-B16	[0.5, 0.5, 0.5]	[0.5, 0.5, 0.5]
ViT-L16	[0.5, 0.5, 0.5]	[0.5, 0.5, 0.5]
DeiT-S16	[0.485, 0.456, 0.406]	[0.229, 0.224, 0.225]
DeiT-B16	[0.485, 0.456, 0.406]	[0.229, 0.224, 0.225]
MLP-Mixer-B16	[0.5, 0.5, 0.5]	[0.5, 0.5, 0.5]
MLP-Mixer-L16	[0.5, 0.5, 0.5]	[0.5, 0.5, 0.5]
ViT-B16 (AugReg)	[0.5, 0.5, 0.5]	[0.5, 0.5, 0.5]
ViT-L16 (AugReg)	[0.5, 0.5, 0.5]	[0.5, 0.5, 0.5]
BeiT-B16	[0.5, 0.5, 0.5]	[0.5, 0.5, 0.5]
BeiT-L16	[0.5, 0.5, 0.5]	[0.5, 0.5, 0.5]

Table 9: MEAN and STD used for data pre-processing on ImageNet, ImageNet-C and ImageNet-Sketch for each backbone network.

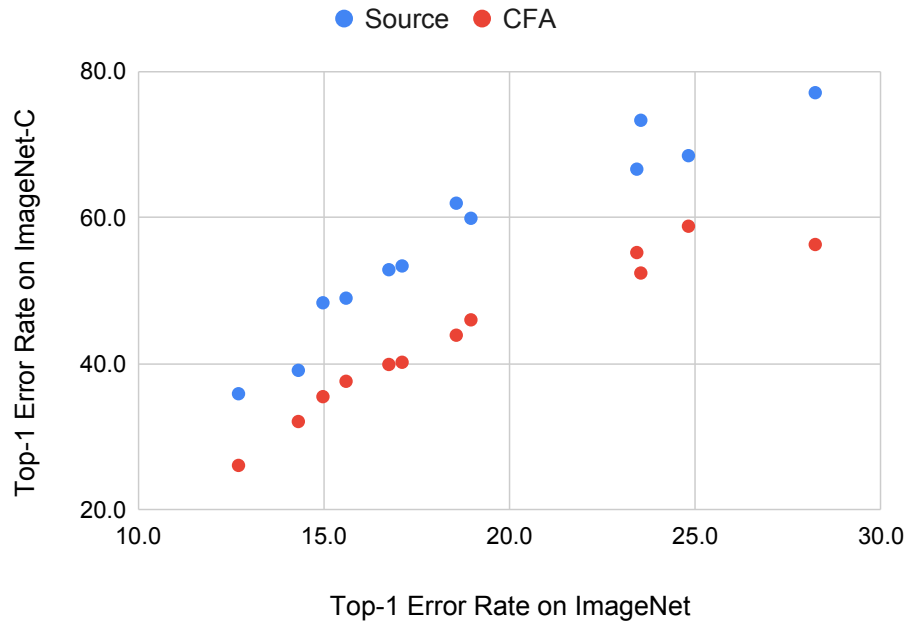


Figure 6: Visualization of model agnosticity study result. Each plot indicates the relationship between the Top-1 error rate on ImageNet (Source dataset) and the Top-1 error rate on ImageNet-C (Target dataset) before / after the CFA adaptation for each backbone network.

Method(Params)	Gaussian	Shot	Impulse	Defocus	Glass	Motion	Zoom	Snow
Source	77.7±0.0	75.1±0.0	77.0±0.0	66.9±0.0	69.1±0.0	58.5±0.0	62.8±0.0	60.9±0.0
Tent(LN)	66.3±8.8	77.8±1.6	59.3±0.2	50.9±0.2	49.8±0.2	46.7±0.0	50.9±0.2	75.7±2.0
Tent(CLS)	74.9±0.1	72.6±0.1	74.4±0.0	63.7±0.2	66.8±0.3	55.8±0.0	61.0±0.0	60.5±0.0
Tent(Feature)	77.0±5.6	87.5±6.0	78.8±3.7	48.8±0.1	47.6±0.1	44.5±0.1	67.5±4.3	84.6±4.4
Tent(ALL)	78.2±7.2	87.8±5.4	79.7±4.6	49.0±0.1	47.7±0.2	44.6±0.1	70.9±4.0	86.7±4.1
PL(LN)	75.5±8.3	71.7±3.7	73.7±8.9	53.2±0.1	52.4±0.1	48.6±0.3	52.4±0.4	75.3±1.8
PL(CLS)	76.3±0.0	74.0±0.1	75.6±0.0	66.4±0.0	68.7±0.0	57.0±0.1	61.8±0.2	60.7±0.0
PL(Feature)	85.5±7.3	85.6±8.7	80.4±9.9	51.6±0.2	50.9±0.1	46.9±0.0	61.3±2.1	88.7±2.5
PL(ALL)	83.6±11.9	90.7±2.8	79.1±13.5	51.7±0.4	51.1±0.4	46.8±0.3	61.1±2.5	88.8±2.3
SHOT-IM(LN)	58.6±0.1	56.4±0.1	57.6±0.1	49.7±0.1	48.7±0.2	46.0±0.1	46.4±0.1	47.0±0.1
SHOT-IM(CLS)	75.5±0.0	73.1±0.0	74.9±0.0	64.5±0.2	68.4±0.0	56.5±0.1	61.4±0.1	60.6±0.0
SHOT-IM(Feature)	57.8±0.2	55.3±0.1	57.1±0.1	47.8±0.1	46.7±0.1	43.7±0.1	44.1±0.2	44.4±0.2
SHOT-IM(ALL)	57.8±0.1	55.3±0.1	57.1±0.2	48.0±0.0	46.8±0.1	43.8±0.1	44.2±0.1	44.4±0.1
CFA(LN)	56.5±0.1	54.2±0.1	55.4±0.1	48.3±0.0	47.1±0.0	44.3±0.0	44.4±0.2	44.9±0.1
CFA(CLS)	74.0±0.1	71.3±0.1	73.5±0.0	60.9±0.2	63.5±0.1	54.9±0.1	60.2±0.0	60.0±0.0
CFA(Feature)	55.1±0.2	52.7±0.1	54.2±0.1	46.7±0.1	44.9±0.1	41.7±0.1	41.5±0.1	42.0±0.1
CFA(ALL)	55.1±0.2	52.7±0.1	54.2±0.1	46.7±0.1	44.9±0.1	41.7±0.1	41.5±0.1	42.0±0.1
Method(Params)	Frost	Fog	Brightness	Contrast	Elastic	Pixelate	Jpeg	Average
Source	57.6±0.0	62.9±0.0	31.6±0.0	88.9±0.0	51.9±0.0	45.3±0.0	42.9±0.0	61.9±0.0
Tent(LN)	48.2±0.4	44.3±0.3	26.1±0.1	58.5±0.3	37.6±0.3	32.7±0.1	34.7±0.1	50.6±0.5
Tent(CLS)	57.2±0.0	56.9±0.2	31.5±0.0	79.4±0.2	51.8±0.0	43.2±0.0	42.1±0.1	59.4±0.0
Tent(Feature)	71.8±6.2	53.2±19.7	25.4±0.1	54.9±0.3	36.6±0.3	30.8±0.0	33.4±0.1	56.2±2.2
Tent(ALL)	71.9±3.8	88.8±1.0	25.4±0.0	54.9±0.3	37.0±0.4	30.8±0.0	33.5±0.1	59.1±1.0
PL(LN)	51.4±0.4	79.5±3.3	26.8±0.1	62.8±0.2	41.1±0.2	35.1±0.2	36.2±0.1	55.7±1.4
PL(CLS)	57.4±0.0	59.0±0.1	31.5±0.0	81.9±0.2	51.9±0.0	44.5±0.1	42.7±0.0	60.6±0.0
PL(Feature)	62.4±10.8	91.6±0.5	26.2±0.1	71.0±10.4	41.0±0.3	33.2±0.2	35.0±0.2	60.8±2.1
PL(ALL)	65.1±11.5	93.8±0.1	26.3±0.1	72.4±11.6	41.6±0.3	33.3±0.1	35.0±0.2	61.4±2.2
SHOT-IM(LN)	45.9±0.1	43.2±0.2	26.1±0.0	56.9±0.2	35.9±0.2	32.4±0.1	34.3±0.1	45.7±0.0
SHOT-IM(CLS)	57.3±0.0	57.3±0.2	31.5±0.0	79.4±0.1	51.8±0.0	44.3±0.0	42.6±0.0	59.9±0.0
SHOT-IM(Feature)	44.3±0.1	40.3±0.1	25.4±0.1	53.2±0.1	34.7±0.1	30.7±0.1	33.2±0.0	43.9±0.0
SHOT-IM(ALL)	44.3±0.1	40.3±0.1	25.4±0.0	53.4±0.2	34.8±0.1	30.7±0.1	33.3±0.1	44.0±0.0
CFA(LN)	44.8±0.1	41.2±0.1	25.6±0.1	54.4±0.2	33.2±0.1	30.5±0.0	33.5±0.1	43.9±0.0
CFA(CLS)	56.6±0.0	56.4±0.1	31.3±0.0	78.0±0.1	50.6±0.1	41.2±0.1	40.1±0.1	58.2±0.0
CFA(Feature)	42.5±0.1	38.1±0.0	24.8±0.1	50.1±0.1	31.8±0.0	28.7±0.0	32.2±0.0	41.8±0.0
CFA(ALL)	42.5±0.1	38.1±0.0	24.8±0.1	50.1±0.1	31.8±0.0	28.7±0.0	32.2±0.0	41.8±0.0

Table 10: Detailed experiment results of Table 1 (Top-1 error rate) based on ViT-B16.

Method(Params)	Gaussian	Shot	Impulse	Defocus	Glass	Motion	Zoom	Snow
Source	60.5±0.0	59.2±0.0	59.1±0.0	61.3±0.0	62.6±0.0	51.0±0.0	54.2±0.0	53.4±0.0
Tent(LN)	48.9±0.1	47.6±0.0	48.0±0.1	46.4±0.1	48.2±0.1	42.0±0.1	44.6±0.1	45.3±0.2
Tent(CLS)	57.9±0.0	56.5±0.0	56.7±0.0	55.3±0.3	58.9±0.3	46.5±0.1	52.1±0.1	51.5±0.1
Tent(Feature)	47.7±0.1	45.7±0.2	46.8±0.2	42.2±0.2	43.2±0.3	38.9±0.1	40.3±0.3	65.8±9.9
Tent(ALL)	47.6±0.1	45.8±0.2	46.8±0.2	42.3±0.2	43.3±0.3	39.0±0.1	40.6±0.3	70.9±5.3
PL(LN)	50.4±0.0	49.0±0.2	49.2±0.2	49.4±0.1	51.6±0.3	43.1±0.1	46.1±0.1	47.7±0.3
PL(CLS)	58.9±0.1	57.5±0.0	57.7±0.1	56.6±0.2	61.3±0.1	47.2±0.3	52.4±0.1	52.3±0.0
PL(Feature)	48.6±0.2	47.2±0.1	48.0±0.1	44.3±0.3	46.0±0.4	40.3±0.2	43.0±1.1	74.2±6.2
PL(ALL)	48.5±0.3	47.3±0.1	47.9±0.1	44.4±0.3	46.2±0.1	40.5±0.2	43.7±1.5	74.5±4.2
SHOT-IM(LN)	48.8±0.0	47.5±0.1	47.9±0.1	45.9±0.0	47.6±0.1	41.7±0.1	43.7±0.1	44.5±0.1
SHOT-IM(CLS)	58.5±0.0	57.2±0.0	57.3±0.0	55.6±0.5	60.4±0.2	46.8±0.1	52.0±0.0	52.0±0.1
SHOT-IM(Feature)	47.3±0.1	45.2±0.0	46.3±0.1	41.9±0.1	42.5±0.2	38.9±0.1	39.3±0.1	40.0±0.1
SHOT-IM(ALL)	47.4±0.1	45.3±0.1	46.3±0.2	41.9±0.1	42.5±0.2	38.9±0.1	39.2±0.1	40.0±0.1
CFA(LN)	47.3±0.0	45.9±0.1	46.4±0.1	44.6±0.1	45.8±0.0	40.3±0.1	41.9±0.1	42.2±0.1
CFA(CLS)	56.7±0.1	55.1±0.1	55.5±0.0	55.4±0.0	56.3±0.3	46.0±0.1	51.1±0.0	50.8±0.1
CFA(Feature)	45.4±0.2	43.5±0.1	44.5±0.2	40.7±0.2	40.8±0.1	37.1±0.2	37.2±0.0	37.6±0.1
CFA(ALL)	45.4±0.2	43.5±0.1	44.5±0.2	40.7±0.2	40.8±0.1	37.1±0.2	37.2±0.0	37.6±0.1
Method(Params)	Frost	Fog	Brightness	Contrast	Elastic	Pixelate	Jpeg	Average
Source	52.6±0.0	57.6±0.0	28.3±0.0	83.8±0.0	45.3±0.0	34.1±0.0	37.5±0.0	53.4±0.0
Tent(LN)	46.3±0.2	41.4±0.1	24.5±0.2	54.2±0.1	37.8±0.2	28.9±0.0	30.9±0.1	42.3±0.0
Tent(CLS)	51.4±0.1	50.5±0.1	28.1±0.0	75.1±0.1	44.6±0.0	33.5±0.0	36.0±0.1	50.3±0.0
Tent(Feature)	80.1±2.7	48.0±18.3	23.2±0.0	46.8±0.1	32.5±0.3	26.4±0.1	29.0±0.2	43.8±0.6
Tent(ALL)	79.6±4.2	49.4±20.6	23.3±0.0	46.7±0.1	32.7±0.3	26.4±0.1	29.0±0.1	44.2±1.1
PL(LN)	48.3±0.2	43.8±0.1	25.2±0.1	57.3±0.2	40.6±0.3	30.2±0.2	32.5±0.0	44.3±0.0
PL(CLS)	52.0±0.0	52.6±0.5	28.2±0.0	76.6±0.1	45.1±0.0	33.8±0.0	36.9±0.2	51.3±0.0
PL(Feature)	69.7±7.7	67.3±14.3	24.0±0.0	50.1±0.2	36.2±0.3	27.8±0.2	30.3±0.3	46.5±0.8
PL(ALL)	72.8±4.8	68.4±15.1	24.0±0.2	50.5±0.3	36.5±0.4	27.8±0.2	30.3±0.2	46.9±0.7
SHOT-IM(LN)	44.5±0.1	40.9±0.1	25.2±0.1	53.4±0.1	36.7±0.2	29.5±0.1	31.5±0.1	42.0±0.0
SHOT-IM(CLS)	51.6±0.1	50.2±0.0	28.2±0.0	74.6±0.0	44.9±0.0	33.8±0.0	36.7±0.0	50.7±0.1
SHOT-IM(Feature)	40.7±0.1	37.1±0.4	23.4±0.1	46.1±0.3	31.2±0.3	26.5±0.2	29.1±0.0	38.4±0.0
SHOT-IM(ALL)	40.7±0.1	37.2±0.4	23.4±0.1	46.0±0.1	31.3±0.2	26.5±0.2	29.1±0.1	38.4±0.0
CFA(LN)	42.4±0.0	38.9±0.1	23.9±0.1	51.8±0.1	33.7±0.1	27.7±0.0	30.1±0.1	40.2±0.0
CFA(CLS)	49.9±0.0	50.1±0.1	27.7±0.0	73.7±0.1	43.0±0.1	32.3±0.1	34.9±0.2	49.2±0.0
CFA(Feature)	38.9±0.0	34.7±0.1	22.6±0.1	43.2±0.1	29.2±0.0	25.5±0.0	28.4±0.0	36.6±0.0
CFA(ALL)	38.9±0.0	34.7±0.1	22.6±0.1	43.2±0.1	29.2±0.0	25.5±0.0	28.4±0.0	36.6±0.0

Table 11: Detailed experiment results of Table 1 (Top-1 error rate) based on ViT-L16.

Method	Gaussian	Shot	Impulse	Defocus	Glass	Motion	Zoom	Snow
C10-C(Source)	23.6±0.0	21.9±0.0	28.7±0.0	5.2±0.0	27.9±0.0	9.1±0.0	4.4±0.0	5.5±0.0
C10-C(Tent)	19.0±0.5	16.8±0.1	36.4±1.7	4.2±0.0	16.8±0.2	6.8±0.1	3.5±0.1	5.1±0.1
C10-C(PL)	20.8±0.1	18.6±0.2	34.4±2.8	4.5±0.1	19.5±0.5	7.6±0.2	3.9±0.1	5.3±0.1
C10-C(TFA)	16.0±0.1	14.4±0.2	14.7±0.2	4.2±0.1	15.5±0.3	6.6±0.1	3.5±0.1	5.0±0.0
C10-C(T3A)	22.2±0.2	20.5±0.1	26.0±0.1	5.3±0.0	25.4±0.1	8.8±0.0	4.4±0.0	5.6±0.0
C10-C(SHOT-IM)	16.8±0.2	15.0±0.2	14.9±0.2	4.2±0.0	15.4±0.2	6.7±0.1	3.5±0.1	4.9±0.0
C10-C(CFA-F)	15.6±0.1	13.9±0.1	14.2±0.2	4.4±0.0	15.1±0.1	6.7±0.1	3.5±0.0	4.9±0.1
C10-C(CFA-C)	15.7±0.1	14.0±0.2	14.5±0.3	4.2±0.1	14.5±0.2	6.2±0.1	3.4±0.1	4.8±0.0
C10-C(CFA)	15.5±0.0	13.8±0.2	14.1±0.3	4.2±0.1	14.5±0.2	6.3±0.2	3.4±0.1	4.7±0.0
C100-C(Source)	55.0±0.0	52.9±0.0	57.8±0.0	18.0±0.0	60.5±0.0	23.6±0.0	16.0±0.0	22.3±0.0
C100-C(Tent)	42.7±0.3	40.0±0.9	47.8±8.5	15.7±0.1	44.9±0.9	19.7±0.1	14.3±0.1	20.4±0.1
C100-C(PL)	45.9±0.4	43.4±1.2	57.8±4.0	16.3±0.3	50.8±0.9	20.8±0.4	14.9±0.2	21.2±0.1
C100-C(TFA)	51.3±0.3	49.4±0.5	49.5±0.8	18.1±0.2	51.8±0.5	23.0±0.5	16.3±0.2	22.9±0.2
C100-C(T3A)	53.6±0.2	51.6±0.1	56.4±0.2	17.8±0.0	56.8±0.1	23.4±0.1	15.9±0.0	21.7±0.1
C100-C(SHOT-IM)	39.4±0.3	37.1±0.2	38.8±0.1	15.7±0.2	38.4±0.1	19.5±0.1	14.4±0.1	20.1±0.0
C100-C(CFA-F)	38.7±0.2	36.2±0.3	37.3±0.3	15.9±0.1	37.4±0.2	19.5±0.1	14.1±0.0	19.9±0.0
C100-C(CFA-C)	39.3±0.4	37.0±0.2	38.3±0.3	15.6±0.1	38.6±0.1	19.5±0.1	14.2±0.1	20.0±0.0
C100-C(CFA)	38.0±0.3	35.9±0.2	36.8±0.3	15.5±0.1	36.9±0.2	19.0±0.2	14.0±0.1	19.6±0.1
IN-C(Source)	77.7±0.0	75.1±0.0	77.0±0.0	66.9±0.0	69.1±0.0	58.5±0.0	62.8±0.0	60.9±0.0
IN-C(Tent)	66.3±8.8	77.8±1.6	59.3±0.2	50.9±0.2	49.8±0.2	46.7±0.0	50.9±0.2	75.7±2.0
IN-C(PL)	75.5±8.3	71.7±3.7	73.7±8.9	53.2±0.1	52.4±0.1	48.6±0.3	52.4±0.4	75.3±1.8
IN-C(TFA)	69.7±0.1	68.0±0.2	69.8±0.2	63.2±0.2	62.6±0.1	57.7±0.1	59.2±0.2	57.0±0.2
IN-C(T3A)	77.8±0.1	74.9±0.1	76.8±0.1	65.5±0.1	68.3±0.0	57.7±0.0	61.7±0.0	60.1±0.0
IN-C(SHOT-IM)	58.6±0.1	56.4±0.1	57.6±0.1	49.7±0.1	48.7±0.2	46.0±0.1	46.4±0.1	47.0±0.1
IN-C(CFA-F)	58.8±0.2	56.7±0.1	57.7±0.1	51.6±0.1	51.5±0.1	47.9±0.1	47.1±0.1	47.0±0.1
IN-C(CFA-C)	58.7±0.1	56.1±0.1	57.5±0.1	50.1±0.1	49.0±0.2	45.6±0.1	46.3±0.2	46.2±0.1
IN-C(CFA)	56.5±0.1	54.2±0.1	55.4±0.1	48.3±0.0	47.1±0.0	44.3±0.0	44.4±0.2	44.9±0.1
Method	Frost	Fog	Brightness	Contrast	Elastic	Pixelate	Jpeg	Average
C10-C(Source)	8.4±0.0	14.2±0.0	2.4±0.0	15.2±0.0	13.9±0.0	25.5±0.0	13.3±0.0	14.6±0.0
C10-C(Tent)	6.0±0.1	8.8±0.2	2.3±0.0	6.5±0.2	10.3±0.2	9.1±0.4	12.2±0.1	10.9±0.2
C10-C(PL)	6.9±0.2	10.5±0.4	2.4±0.0	7.9±0.4	11.6±0.4	11.9±1.2	12.4±0.3	11.9±0.0
C10-C(TFA)	5.7±0.0	8.0±0.0	2.2±0.0	6.1±0.1	10.1±0.1	7.7±0.1	12.2±0.1	8.8±0.0
C10-C(T3A)	8.0±0.0	13.5±0.0	2.5±0.0	14.1±0.0	13.4±0.0	22.9±0.2	13.5±0.0	13.7±0.0
C10-C(SHOT-IM)	5.8±0.1	8.0±0.2	2.3±0.0	6.1±0.1	10.0±0.1	8.1±0.0	11.8±0.1	8.9±0.0
C10-C(CFA-F)	5.6±0.1	8.1±0.1	2.2±0.0	6.3±0.1	9.6±0.0	7.7±0.1	12.6±0.1	8.7±0.0
C10-C(CFA-C)	5.5±0.0	7.6±0.1	2.2±0.1	5.7±0.1	9.3±0.0	7.4±0.1	12.1±0.2	8.5±0.0
C10-C(CFA)	5.5±0.1	7.6±0.0	2.1±0.0	5.8±0.1	9.2±0.1	7.4±0.2	12.1±0.1	8.4±0.0
C100-C(Source)	27.5±0.0	34.2±0.0	11.9±0.0	35.3±0.0	34.8±0.0	43.3±0.0	33.7±0.0	35.1±0.0
C100-C(Tent)	21.5±0.4	28.0±0.2	11.2±0.1	22.1±0.4	27.9±0.2	22.9±0.6	31.5±0.3	27.4±0.5
C100-C(PL)	23.6±0.4	29.8±0.0	11.6±0.1	25.6±0.6	30.6±0.3	26.8±1.3	32.3±0.4	30.1±0.5
C100-C(TFA)	24.1±0.2	34.0±0.2	12.9±0.2	27.5±1.0	34.3±0.8	31.7±0.9	35.7±0.1	32.2±0.2
C100-C(T3A)	26.3±0.1	33.0±0.1	11.9±0.0	33.7±0.1	33.4±0.1	41.2±0.2	33.3±0.1	34.0±0.0
C100-C(SHOT-IM)	20.8±0.2	26.8±0.2	11.2±0.1	21.5±0.3	27.2±0.1	22.3±0.2	30.5±0.2	25.6±0.0
C100-C(CFA-F)	20.2±0.1	25.9±0.1	11.2±0.1	21.9±0.1	26.1±0.2	21.5±0.2	32.1±0.0	25.2±0.0
C100-C(CFA-C)	20.2±0.2	26.2±0.2	11.1±0.1	20.6±0.4	26.9±0.1	21.6±0.1	31.0±0.2	25.3±0.1
C100-C(CFA)	19.7±0.1	25.3±0.2	10.8±0.1	20.4±0.3	25.8±0.2	20.9±0.2	31.2±0.3	24.6±0.1
IN-C(Source)	57.6±0.0	62.9±0.0	31.6±0.0	88.9±0.0	51.9±0.0	45.3±0.0	42.9±0.0	61.9±0.0
IN-C(Tent)	48.2±0.4	44.3±0.3	26.1±0.1	58.5±0.3	37.6±0.3	32.7±0.1	34.7±0.1	50.6±0.5
IN-C(PL)	51.4±0.4	79.5±3.3	26.8±0.1	62.8±0.2	41.1±0.2	35.1±0.2	36.2±0.1	55.7±1.4
IN-C(TFA)	55.1±0.1	58.3±0.1	34.7±0.1	74.8±0.2	45.9±0.0	45.5±0.1	45.1±0.0	57.8±0.1
IN-C(T3A)	56.8±0.0	62.0±0.0	30.7±0.1	89.4±0.1	49.9±0.0	44.7±0.0	41.7±0.0	61.2±0.0
IN-C(SHOT-IM)	45.9±0.1	43.2±0.2	26.1±0.0	56.9±0.2	35.9±0.2	32.4±0.1	34.3±0.1	45.7±0.0
IN-C(CFA-F)	47.0±0.1	44.4±0.1	27.0±0.0	58.9±0.1	35.4±0.0	33.4±0.0	35.5±0.0	46.7±0.0
IN-C(CFA-C)	45.6±0.1	41.9±0.2	26.1±0.1	56.3±0.2	34.7±0.0	31.5±0.1	34.2±0.0	45.3±0.0
IN-C(CFA)	44.8±0.1	41.2±0.1	25.6±0.1	54.4±0.2	33.2±0.1	30.5±0.0	33.5±0.1	43.9±0.0

Table 12: Detailed experiment results of Table 2 (Top-1 error rate) for each methods on CIFAR-10-C, CIFAR-100-C and ImageNet-C with severity level=5 by ViT-B16 model.

Method	Gaussian	Shot	Impulse	Defocus	Glass	Motion	Zoom	Snow
ResNet50	97.8±0.0	97.1±0.0	98.1±0.0	82.1±0.0	90.2±0.0	85.2±0.0	77.5±0.0	83.1±0.0
ResNet101	96.5±0.0	95.7±0.0	96.5±0.0	78.1±0.0	86.8±0.0	80.8±0.0	73.5±0.0	79.0±0.0
ViT-B16	77.7±0.0	75.1±0.0	77.0±0.0	66.9±0.0	69.1±0.0	58.5±0.0	62.8±0.0	60.9±0.0
ViT-L16	60.5±0.0	59.2±0.0	59.1±0.0	61.3±0.0	62.6±0.0	51.0±0.0	54.2±0.0	53.4±0.0
DeiT-S16	69.6±0.0	67.6±0.0	68.1±0.0	72.4±0.0	81.8±0.0	65.2±0.0	70.9±0.0	51.4±0.0
DeiT-B16	58.0±0.0	57.6±0.0	57.0±0.0	66.7±0.0	76.8±0.0	60.8±0.0	65.2±0.0	45.0±0.0
MLP-Mixer-B16	85.0±0.0	84.6±0.0	87.1±0.0	82.3±0.0	88.3±0.0	72.7±0.0	77.0±0.0	67.6±0.0
MLP-Mixer-L16	82.8±0.0	84.9±0.0	85.8±0.0	86.0±0.0	90.2±0.0	80.3±0.0	80.2±0.0	79.0±0.0
ViT-B16 (AugReg)	53.1±0.0	52.4±0.0	53.1±0.0	57.3±0.0	65.8±0.0	49.6±0.0	55.3±0.0	43.1±0.0
ViT-L16 (AugReg)	37.9±0.0	38.6±0.0	37.7±0.0	47.3±0.0	54.9±0.0	39.4±0.0	44.9±0.0	33.8±0.0
BeiT-B16	52.8±0.0	49.9±0.0	50.5±0.0	57.7±0.0	65.9±0.0	50.4±0.0	57.0±0.0	41.8±0.0
BeiT-L16	36.5±0.0	35.1±0.0	35.0±0.0	42.5±0.0	53.0±0.0	36.7±0.0	43.1±0.0	29.8±0.0
Method	Frost	Fog	Brightness	Contrast	Elastic	Pixelate	Jpeg	Average
ResNet50	76.7±0.0	75.6±0.0	41.1±0.0	94.6±0.0	83.1±0.0	79.4±0.0	68.3±0.0	82.0±0.0
ResNet101	73.3±0.0	71.9±0.0	38.6±0.0	92.8±0.0	75.7±0.0	65.0±0.0	57.6±0.0	77.4±0.0
ViT-B16	57.6±0.0	62.9±0.0	31.6±0.0	88.9±0.0	51.9±0.0	45.3±0.0	42.9±0.0	61.9±0.0
ViT-L16	52.6±0.0	57.6±0.0	28.3±0.0	83.8±0.0	45.3±0.0	34.1±0.0	37.5±0.0	53.4±0.0
DeiT-S16	49.1±0.0	41.6±0.0	27.4±0.0	52.5±0.0	66.9±0.0	65.2±0.0	48.6±0.0	59.9±0.0
DeiT-B16	42.6±0.0	37.1±0.0	24.0±0.0	45.2±0.0	64.1±0.0	51.1±0.0	41.5±0.0	52.9±0.0
MLP-Mixer-B16	59.1±0.0	62.0±0.0	35.8±0.0	88.3±0.0	75.4±0.0	71.6±0.0	62.4±0.0	73.3±0.0
MLP-Mixer-L16	65.0±0.0	63.0±0.0	43.8±0.0	87.6±0.0	75.3±0.0	82.7±0.0	69.1±0.0	77.1±0.0
ViT-B16 (AugReg)	47.4±0.0	43.5±0.0	23.9±0.0	68.2±0.0	53.3±0.0	34.5±0.0	34.0±0.0	49.0±0.0
ViT-L16 (AugReg)	37.6±0.0	37.5±0.0	19.8±0.0	60.1±0.0	43.8±0.0	25.7±0.0	27.3±0.0	39.1±0.0
BeiT-B16	48.5±0.0	52.5±0.0	23.3±0.0	47.8±0.0	57.7±0.0	36.1±0.0	33.1±0.0	48.3±0.0
BeiT-L16	37.0±0.0	37.6±0.0	18.5±0.0	33.5±0.0	46.8±0.0	27.0±0.0	26.4±0.0	35.9±0.0

Table 13: Detailed experiment results of Table 3 (Top-1 error rate) by Source.

Method	Gaussian	Shot	Impulse	Defocus	Glass	Motion	Zoom	Snow
ResNet50	74.2±0.1	72.2±0.1	73.4±0.1	74.4±0.1	74.7±0.3	61.5±0.1	52.0±0.1	54.7±0.1
ResNet101	71.2±0.1	68.7±0.1	70.8±0.0	70.8±0.2	70.5±0.2	57.9±0.1	48.8±0.0	51.7±0.1
ViT-B16	58.6±0.1	56.4±0.1	57.7±0.1	49.8±0.2	48.7±0.2	45.9±0.1	46.4±0.1	47.0±0.1
ViT-L16	48.8±0.0	47.5±0.1	47.9±0.1	45.9±0.0	47.6±0.1	41.7±0.1	43.8±0.1	44.5±0.1
DeiT-S16	54.4±0.2	52.4±0.1	53.3±0.1	57.3±0.1	56.1±0.1	48.9±0.1	51.4±0.0	42.6±0.0
DeiT-B16	43.7±0.1	42.6±0.1	42.5±0.1	52.0±0.1	49.9±0.0	43.6±0.2	45.8±0.2	36.1±0.0
MLP-Mixer-B16	66.2±0.1	65.4±0.2	65.7±0.3	65.4±0.1	65.4±0.5	55.8±0.2	55.7±0.1	51.0±0.3
MLP-Mixer-L16	65.8±0.2	65.6±0.1	66.6±0.2	72.7±0.4	73.8±0.4	62.7±0.0	66.0±0.2	60.9±0.0
ViT-B16 (AugReg)	43.4±0.0	42.3±0.0	42.4±0.1	44.1±0.1	48.5±0.0	40.9±0.1	43.9±0.1	35.3±0.2
ViT-L16 (AugReg)	34.0±0.0	32.9±0.1	33.4±0.1	38.2±0.1	43.3±0.2	34.3±0.1	38.2±0.0	30.6±0.0
BeiT-B16	43.3±0.1	40.9±0.0	41.9±0.1	44.9±0.1	46.2±0.1	40.0±0.1	43.8±0.1	35.1±0.0
BeiT-L16	30.6±0.0	29.4±0.0	29.7±0.0	34.1±0.1	36.9±0.2	30.3±0.1	34.0±0.1	25.3±0.1
Method	Frost	Fog	Brightness	Contrast	Elastic	Pixelate	Jpeg	Average
ResNet50	59.7±0.1	43.6±0.1	32.8±0.1	70.5±0.2	46.2±0.1	42.4±0.1	49.1±0.0	58.8±0.0
ResNet101	56.6±0.1	42.0±0.1	31.2±0.0	67.2±0.1	42.5±0.1	39.8±0.1	45.9±0.1	55.7±0.0
ViT-B16	45.9±0.1	43.2±0.2	26.1±0.0	56.9±0.2	35.9±0.2	32.4±0.1	34.4±0.1	45.7±0.0
ViT-L16	44.5±0.1	40.9±0.1	25.2±0.1	53.4±0.1	36.7±0.1	29.5±0.1	31.5±0.1	42.0±0.0
DeiT-S16	43.4±0.1	35.3±0.1	26.1±0.0	41.3±0.1	47.1±0.1	42.6±0.1	39.7±0.1	46.1±0.0
DeiT-B16	39.4±0.1	31.1±0.0	23.1±0.0	35.5±0.1	43.0±0.2	35.6±0.1	34.8±0.1	39.9±0.0
MLP-Mixer-B16	51.4±0.3	47.5±0.6	31.2±0.1	60.7±0.3	49.9±0.1	46.6±0.2	48.3±0.2	55.1±0.1
MLP-Mixer-L16	63.0±0.7	57.7±0.1	39.9±0.2	70.5±0.2	59.3±0.6	55.1±0.5	56.6±0.2	62.4±0.1
ViT-B16 (AugReg)	37.4±0.1	33.8±0.1	22.4±0.0	42.0±0.2	39.2±0.0	29.8±0.1	31.5±0.1	38.4±0.0
ViT-L16 (AugReg)	33.3±0.1	32.5±0.1	19.3±0.0	41.5±0.0	37.0±0.1	23.9±0.0	26.2±0.2	33.3±0.0
BeiT-B16	39.0±0.1	35.4±0.1	21.8±0.1	33.0±0.2	39.0±0.1	30.2±0.1	29.4±0.0	37.6±0.0
BeiT-L16	30.3±0.0	26.7±0.1	16.7±0.0	23.6±0.1	30.8±0.1	21.5±0.1	22.9±0.0	28.2±0.0

Table 14: Detailed experiment results of Table 3 (Top-1 error rate) by SHOT-IM.

Method	Gaussian	Shot	Impulse	Defocus	Glass	Motion	Zoom	Snow
ResNet50	74.6±0.0	73.7±0.1	73.7±0.2	74.6±0.1	75.0±0.1	61.4±0.1	52.1±0.0	54.3±0.1
ResNet101	70.8±0.1	68.5±0.1	70.5±0.1	70.6±0.2	70.2±0.1	57.5±0.2	48.7±0.0	51.1±0.0
ViT-B16	56.5±0.1	54.1±0.1	55.4±0.1	48.4±0.0	47.1±0.0	44.3±0.0	44.4±0.2	44.9±0.1
ViT-L16	47.3±0.0	45.9±0.1	46.4±0.1	44.6±0.1	45.8±0.0	40.3±0.1	41.9±0.0	42.2±0.1
DeiT-S16	54.5±0.1	52.4±0.1	53.5±0.1	58.0±0.1	56.8±0.2	49.5±0.1	51.4±0.1	41.9±0.1
DeiT-B16	44.5±0.1	42.9±0.1	43.3±0.0	54.2±0.1	53.3±0.1	44.3±0.1	45.4±0.2	34.1±0.1
MLP-Mixer-B16	63.9±0.1	62.5±0.1	63.3±0.0	64.5±0.1	66.4±0.2	54.3±0.2	54.1±0.2	46.3±0.1
MLP-Mixer-L16	61.1±0.1	60.1±0.3	61.8±0.1	70.6±0.1	69.7±0.1	57.9±0.2	58.7±0.2	52.0±0.2
ViT-B16 (AugReg)	43.1±0.0	42.0±0.1	41.9±0.1	45.6±0.0	51.1±0.2	40.1±0.0	43.3±0.1	33.6±0.2
ViT-L16 (AugReg)	33.6±0.1	32.8±0.1	33.3±0.1	38.1±0.1	42.5±0.2	34.2±0.2	36.5±0.1	28.6±0.0
BeiT-B16	41.9±0.1	39.5±0.1	40.5±0.1	43.2±0.0	44.2±0.1	37.7±0.1	41.2±0.1	32.7±0.0
BeiT-L16	29.5±0.1	28.0±0.1	28.5±0.0	32.0±0.0	33.7±0.1	27.7±0.1	30.2±0.0	23.9±0.0
Method	Frost	Fog	Brightness	Contrast	Elastic	Pixelate	Jpeg	Average
ResNet50	59.5±0.1	43.8±0.0	33.2±0.1	68.6±0.2	46.2±0.1	42.4±0.2	49.2±0.1	58.8±0.0
ResNet101	56.0±0.1	41.9±0.1	31.4±0.1	64.4±0.2	42.2±0.2	39.7±0.1	45.7±0.1	55.3±0.1
ViT-B16	44.8±0.1	41.1±0.1	25.6±0.1	54.4±0.3	33.3±0.1	30.6±0.0	33.5±0.1	43.9±0.0
ViT-L16	42.4±0.0	38.9±0.1	23.9±0.1	51.8±0.1	33.7±0.1	27.7±0.0	30.1±0.1	40.2±0.0
DeiT-S16	42.9±0.1	38.5±0.2	25.0±0.0	41.3±0.1	46.0±0.1	40.8±0.1	38.2±0.0	46.0±0.0
DeiT-B16	37.4±0.0	35.2±0.2	21.7±0.0	34.2±0.0	41.0±0.1	34.1±0.0	32.8±0.1	39.9±0.0
MLP-Mixer-B16	46.8±0.1	42.5±0.3	29.3±0.1	53.3±0.1	48.7±0.5	44.8±0.3	45.7±0.1	52.4±0.1
MLP-Mixer-L16	55.2±0.3	48.6±0.0	33.9±0.1	60.6±0.6	52.3±0.3	49.2±0.1	52.5±0.1	56.3±0.0
ViT-B16 (AugReg)	35.9±0.2	32.3±0.0	21.0±0.0	41.2±0.1	35.7±0.1	28.3±0.0	29.8±0.1	37.6±0.0
ViT-L16 (AugReg)	31.0±0.1	30.7±0.0	18.1±0.0	41.4±0.3	32.8±0.1	22.2±0.1	25.4±0.1	32.1±0.0
BeiT-B16	37.1±0.1	33.4±0.1	19.7±0.1	31.0±0.1	35.1±0.1	27.3±0.1	26.9±0.0	35.4±0.0
BeiT-L16	28.8±0.1	24.4±0.1	15.7±0.0	22.1±0.0	26.4±0.1	19.4±0.0	20.7±0.0	26.0±0.0

Table 15: Detailed experiment results of Table 3 (Top-1 error rate) by CFA.

Method	Gaussian	Shot	Impulse	Defocus	Glass	Motion	Zoom	Snow
Source (s=1)	16.8±0.0	16.7±0.0	16.8±0.0	17.4±0.0	17.5±0.0	15.3±0.0	19.9±0.0	17.9±0.0
Source (s=2)	17.9±0.0	18.2±0.0	18.4±0.0	19.9±0.0	20.7±0.0	17.1±0.0	24.3±0.0	23.5±0.0
Source (s=3)	20.3±0.0	20.5±0.0	19.9±0.0	26.1±0.0	35.3±0.0	21.6±0.0	29.6±0.0	23.0±0.0
Source (s=4)	25.5±0.0	27.0±0.0	25.5±0.0	33.6±0.0	40.9±0.0	29.5±0.0	34.7±0.0	27.1±0.0
Source (s=5)	36.5±0.0	35.1±0.0	35.0±0.0	42.5±0.0	53.0±0.0	36.7±0.0	43.1±0.0	29.8±0.0
Tent (s=1)	15.3±0.1	15.4±0.0	15.7±0.0	15.4±0.0	15.7±0.0	14.5±0.1	18.1±0.0	16.4±0.0
Tent (s=2)	16.4±0.0	16.6±0.0	17.1±0.0	17.0±0.0	17.8±0.1	16.1±0.0	21.1±0.1	20.6±0.0
Tent (s=3)	18.6±0.0	18.7±0.0	18.6±0.0	21.2±0.0	25.4±0.1	19.5±0.1	24.9±0.0	20.4±0.0
Tent (s=4)	22.5±0.1	23.5±0.0	22.7±0.0	26.6±0.0	28.8±0.1	24.9±0.1	28.0±0.0	23.4±0.1
Tent (s=5)	29.9±0.0	28.6±0.1	29.2±0.1	33.7±0.1	36.5±0.2	29.6±0.1	33.8±0.1	24.8±0.1
SHOT-IM (s=1)	15.8±0.0	15.9±0.0	16.1±0.0	15.7±0.0	16.2±0.0	14.7±0.0	18.6±0.0	16.7±0.0
SHOT-IM (s=2)	16.6±0.0	17.0±0.0	17.4±0.0	17.5±0.0	18.6±0.0	16.3±0.0	21.9±0.1	21.1±0.0
SHOT-IM (s=3)	18.9±0.0	19.1±0.0	18.9±0.0	21.7±0.0	26.8±0.1	20.0±0.0	25.7±0.0	21.0±0.1
SHOT-IM (s=4)	23.2±0.1	24.2±0.1	23.3±0.0	27.2±0.1	30.1±0.1	25.6±0.1	28.8±0.0	24.0±0.0
SHOT-IM (s=5)	30.6±0.0	29.4±0.0	29.7±0.0	34.1±0.1	36.9±0.2	30.3±0.1	34.0±0.1	25.3±0.1
CFA (s=1)	15.2±0.1	15.2±0.0	15.7±0.0	15.3±0.0	15.4±0.0	14.6±0.1	17.6±0.1	16.2±0.0
CFA (s=2)	16.3±0.1	16.5±0.0	17.0±0.1	16.8±0.1	17.2±0.1	15.9±0.1	20.1±0.0	20.0±0.1
CFA (s=3)	18.4±0.0	18.6±0.1	18.4±0.1	20.5±0.0	23.6±0.0	19.0±0.0	23.1±0.1	19.7±0.0
CFA (s=4)	22.3±0.1	23.1±0.1	22.4±0.1	25.6±0.1	26.7±0.1	23.5±0.1	25.8±0.1	22.7±0.1
CFA (s=5)	29.5±0.1	28.0±0.1	28.5±0.0	32.0±0.0	33.7±0.1	27.7±0.1	30.2±0.0	23.9±0.0
Method	Frost	Fog	Brightness	Contrast	Elastic	Pixelate	Jpeg	Average
Source (s=1)	18.1±0.0	17.8±0.0	14.4±0.0	14.7±0.0	17.5±0.0	15.7±0.0	16.2±0.0	16.8±0.0
Source (s=2)	24.5±0.0	19.5±0.0	15.0±0.0	15.1±0.0	36.1±0.0	16.9±0.0	17.5±0.0	20.3±0.0
Source (s=3)	30.6±0.0	22.8±0.0	15.8±0.0	16.3±0.0	18.9±0.0	17.7±0.0	18.5±0.0	22.5±0.0
Source (s=4)	32.1±0.0	26.9±0.0	16.7±0.0	20.9±0.0	24.6±0.0	20.5±0.0	21.7±0.0	27.2±0.0
Source (s=5)	37.0±0.0	37.6±0.0	18.5±0.0	33.5±0.0	46.8±0.0	27.0±0.0	26.4±0.0	35.9±0.0
Tent (s=1)	16.3±0.1	15.9±0.0	13.4±0.0	14.0±0.1	15.8±0.0	14.2±0.0	15.0±0.0	15.4±0.0
Tent (s=2)	21.2±0.0	16.8±0.0	13.8±0.0	14.3±0.0	29.6±0.0	14.7±0.0	15.8±0.1	17.9±0.0
Tent (s=3)	30.9±6.4	18.6±0.1	14.4±0.0	15.1±0.0	16.6±0.0	15.7±0.0	16.3±0.1	19.6±0.4
Tent (s=4)	50.2±17.7	20.9±0.1	15.0±0.1	17.4±0.0	19.5±0.0	17.8±0.1	18.5±0.0	24.0±1.2
Tent (s=5)	75.5±3.4	26.1±0.0	16.0±0.1	23.0±0.0	75.4±4.0	20.3±0.1	21.5±0.0	33.6±0.1
SHOT-IM (s=1)	16.6±0.0	16.4±0.1	13.6±0.1	14.2±0.0	16.2±0.0	14.4±0.0	15.5±0.0	15.8±0.0
SHOT-IM (s=2)	21.6±0.0	17.4±0.0	14.0±0.1	14.6±0.0	30.1±0.1	15.1±0.1	16.4±0.1	18.4±0.0
SHOT-IM (s=3)	25.9±0.1	19.4±0.0	14.6±0.0	15.4±0.0	17.3±0.0	16.1±0.0	17.0±0.0	19.9±0.0
SHOT-IM (s=4)	27.0±0.1	21.6±0.0	15.4±0.1	18.1±0.1	20.8±0.0	18.6±0.1	19.5±0.1	23.2±0.0
SHOT-IM (s=5)	30.3±0.0	26.7±0.1	16.7±0.0	23.6±0.1	30.8±0.1	21.5±0.1	22.9±0.0	28.2±0.0
CFA (s=1)	16.1±0.1	15.6±0.0	13.5±0.1	14.0±0.0	15.6±0.0	14.2±0.0	14.8±0.0	15.3±0.0
CFA (s=2)	20.4±0.0	16.3±0.0	13.8±0.1	14.4±0.0	27.7±0.0	14.4±0.0	15.5±0.1	17.5±0.0
CFA (s=3)	24.4±0.1	17.8±0.0	14.2±0.0	14.9±0.0	16.1±0.0	15.4±0.0	16.0±0.0	18.7±0.0
CFA (s=4)	25.5±0.1	19.7±0.1	14.9±0.0	16.8±0.0	18.1±0.0	17.3±0.1	17.7±0.1	21.5±0.0
CFA (s=5)	28.8±0.1	24.4±0.1	15.7±0.0	22.1±0.0	26.4±0.1	19.4±0.0	20.7±0.0	26.0±0.0

Table 16: Detailed experiment results of Table 4 (Top-1 error rate).

Method	Gaussian	Shot	Impulse	Defocus	Glass	Motion	Zoom	Snow
Tent (LR=0.01)	96.1±1.8	95.6±1.2	93.4±5.9	66.6±5.7	70.6±11.5	67.8±13.0	87.6±3.0	96.5±1.0
Tent (LR=0.0001)	69.1±0.3	66.8±0.0	68.2±0.1	62.1±0.1	63.0±0.1	53.8±0.1	57.6±0.1	56.2±0.1
Tent (BS=32)	71.7±5.5	81.9±0.6	63.3±8.0	49.8±0.4	48.3±0.1	45.7±0.1	56.2±4.1	83.2±3.0
Tent (BS=128)	62.5±1.1	67.4±4.6	61.2±0.7	52.5±0.1	51.6±0.3	47.7±0.0	51.2±0.1	62.9±5.1
Tent (GC=OFF)	97.3±0.3	92.0±2.6	94.9±3.9	53.9±3.5	59.6±16.1	50.9±1.3	85.9±0.8	93.2±5.2
CFA (LR=0.01)	54.0±0.3	51.4±0.3	52.9±0.1	47.3±0.2	44.6±0.3	40.8±0.0	40.3±0.1	41.1±0.3
CFA (LR=0.0001)	66.3±0.2	63.7±0.1	65.2±0.1	57.7±0.0	59.4±0.0	51.6±0.0	54.0±0.1	53.4±0.1
CFA (BS=32)	55.6±0.1	53.2±0.1	54.6±0.1	47.5±0.2	46.2±0.1	43.4±0.1	43.4±0.2	44.1±0.1
CFA (BS=128)	58.2±0.1	55.8±0.1	57.2±0.1	50.0±0.1	49.0±0.0	45.8±0.0	46.1±0.1	46.4±0.1
CFA (GC=OFF)	53.9±0.2	51.5±0.2	52.8±0.1	46.6±0.1	44.6±0.2	41.2±0.1	40.9±0.0	41.6±0.1
CFA ($\lambda=0.5$)	56.5±0.1	54.2±0.1	55.5±0.1	48.7±0.0	47.4±0.1	44.6±0.1	44.6±0.2	44.9±0.1
CFA ($\lambda=2.0$)	56.8±0.2	54.5±0.0	55.9±0.1	48.6±0.1	47.5±0.1	44.5±0.1	44.7±0.2	45.1±0.1
Method	Frost	Fog	Brightness	Contrast	Elastic	Pixelate	Jpeg	Average
Tent (LR=0.01)	89.9±2.6	91.1±2.5	26.1±0.2	84.0±3.4	35.5±3.6	30.2±0.2	33.8±0.4	71.0±1.5
Tent (LR=0.0001)	54.7±0.1	55.1±0.0	29.3±0.1	76.8±0.2	48.4±0.1	41.2±0.0	40.0±0.1	56.2±0.0
Tent (BS=32)	47.6±0.9	42.9±0.2	25.7±0.1	56.5±0.5	35.9±0.4	31.5±0.1	34.0±0.2	51.6±0.8
Tent (BS=128)	49.3±0.1	46.1±0.2	26.5±0.1	62.1±0.1	39.6±0.3	34.3±0.0	35.5±0.1	50.0±0.6
Tent (GC=OFF)	83.5±2.5	84.9±7.4	25.5±0.0	85.2±8.6	33.4±0.5	29.8±0.0	33.1±0.1	66.9±1.5
CFA (LR=0.01)	42.9±0.2	36.6±0.0	25.4±0.1	46.6±0.3	30.7±0.1	28.5±0.0	32.4±0.1	41.0±0.1
CFA (LR=0.0001)	51.8±0.0	52.4±0.1	28.3±0.0	73.1±0.1	44.4±0.0	39.0±0.1	38.2±0.1	53.2±0.0
CFA (BS=32)	44.1±0.1	39.8±0.0	25.5±0.1	52.0±0.0	32.4±0.0	29.8±0.1	33.0±0.1	43.0±0.0
CFA (BS=128)	45.9±0.1	43.4±0.1	26.0±0.0	57.8±0.1	35.1±0.1	32.0±0.1	34.3±0.1	45.5±0.0
CFA (GC=OFF)	42.5±0.2	36.9±0.1	25.3±0.1	46.9±0.1	30.8±0.1	28.6±0.1	32.1±0.1	41.1±0.0
CFA ($\lambda=0.5$)	45.0±0.0	41.4±0.0	25.6±0.1	54.6±0.2	33.3±0.1	30.8±0.0	33.7±0.1	44.1±0.0
CFA ($\lambda=2.0$)	44.8±0.0	41.2±0.1	25.7±0.1	54.5±0.2	33.5±0.1	30.7±0.0	33.6±0.1	44.1±0.0

Table 17: Detailed experiment results of Figure 1 (Top-1 error rate).

Method	Gaussian	Shot	Impulse	Defocus	Glass	Motion	Zoom	Snow
CFA-F ($K=1$) (<i>h</i>)	58.9±0.1	56.7±0.1	57.7±0.1	51.6±0.0	51.6±0.0	48.0±0.1	47.1±0.1	47.0±0.1
CFA-F ($K=1$) (<i>f</i>)	58.6±0.1	56.5±0.0	57.5±0.1	51.5±0.1	51.8±0.2	47.7±0.0	46.8±0.1	46.7±0.1
CFA-F ($K=3$) (<i>h</i>)	58.8±0.2	56.7±0.1	57.7±0.1	51.6±0.1	51.5±0.1	47.9±0.1	47.1±0.1	47.0±0.1
CFA-F ($K=3$) (<i>f</i>)	59.4±0.3	57.1±0.2	58.4±0.3	51.5±0.1	52.5±0.3	48.4±0.0	47.8±0.2	47.9±0.1
CFA-F ($K=5$) (<i>h</i>)	58.8±0.2	56.7±0.1	57.6±0.1	51.6±0.1	51.5±0.0	47.8±0.0	47.0±0.1	47.1±0.1
CFA-F ($K=5$) (<i>f</i>)	66.1±0.3	64.0±0.2	65.5±0.2	59.1±0.2	62.1±1.4	53.5±0.2	55.9±0.5	56.4±0.5
CFA-C (<i>h</i>)	58.7±0.1	56.1±0.1	57.5±0.1	50.1±0.1	49.0±0.2	45.6±0.1	46.3±0.2	46.2±0.1
CFA-C (<i>f</i>)	60.7±1.1	58.8±0.2	59.1±1.0	52.0±0.2	50.9±0.0	46.8±0.1	47.0±0.3	47.0±0.0
CFA ($K=1$) (<i>h</i>)	56.6±0.1	54.3±0.2	55.6±0.1	48.5±0.0	47.2±0.1	44.4±0.0	44.5±0.2	45.0±0.1
CFA ($K=1$) (<i>f</i>)	57.3±0.0	54.9±0.0	56.2±0.1	50.4±0.1	49.7±0.0	45.8±0.0	45.5±0.1	45.7±0.1
CFA ($K=3$) (<i>h</i>)	56.5±0.1	54.2±0.1	55.4±0.1	48.3±0.0	47.1±0.0	44.3±0.0	44.4±0.2	44.9±0.1
CFA ($K=3$) (<i>f</i>)	57.2±0.1	54.9±0.0	56.1±0.1	48.5±0.1	48.1±0.1	44.9±0.1	45.2±0.1	45.6±0.0
CFA ($K=5$) (<i>h</i>)	56.4±0.1	54.2±0.1	55.5±0.1	48.4±0.1	47.2±0.1	44.4±0.0	44.4±0.2	44.9±0.1
CFA ($K=5$) (<i>f</i>)	64.6±0.3	62.0±0.1	63.5±0.1	55.7±0.3	58.7±0.8	51.3±0.2	53.4±0.2	54.0±0.3
Method	Frost	Fog	Brightness	Contrast	Elastic	Pixelate	Jpeg	Average
CFA-F ($K=1$) (<i>h</i>)	47.0±0.1	44.4±0.1	27.0±0.0	58.9±0.1	35.4±0.0	33.4±0.0	35.6±0.0	46.7±0.0
CFA-F ($K=1$) (<i>f</i>)	46.8±0.0	44.2±0.1	26.8±0.0	61.7±0.4	35.2±0.0	33.2±0.1	35.3±0.0	46.7±0.0
CFA-F ($K=3$) (<i>h</i>)	47.0±0.1	44.4±0.1	27.0±0.0	58.9±0.1	35.4±0.0	33.4±0.0	35.5±0.0	46.7±0.0
CFA-F ($K=3$) (<i>f</i>)	47.4±0.1	45.6±0.1	27.1±0.1	59.9±0.3	36.6±0.1	34.0±0.3	35.6±0.1	47.3±0.0
CFA-F ($K=5$) (<i>h</i>)	47.0±0.1	44.4±0.0	27.0±0.0	58.8±0.2	35.4±0.0	33.4±0.0	35.5±0.0	46.6±0.0
CFA-F ($K=5$) (<i>f</i>)	53.4±0.5	53.5±0.3	29.4±0.4	72.6±0.3	45.8±0.1	40.7±0.4	39.7±0.3	54.5±0.1
CFA-C (<i>h</i>)	45.6±0.1	41.9±0.2	26.1±0.1	56.3±0.2	34.7±0.0	31.5±0.1	34.2±0.0	45.3±0.0
CFA-C (<i>f</i>)	46.7±0.1	43.0±0.2	26.5±0.1	65.9±0.1	35.4±0.0	32.0±0.1	35.0±0.0	47.1±0.1
CFA ($K=1$) (<i>h</i>)	44.9±0.0	41.2±0.1	25.6±0.1	54.4±0.1	33.3±0.1	30.6±0.0	33.6±0.1	44.0±0.0
CFA ($K=1$) (<i>f</i>)	45.3±0.1	41.7±0.2	26.3±0.0	60.6±0.2	34.2±0.1	31.2±0.0	34.5±0.1	45.3±0.0
CFA ($K=3$) (<i>h</i>)	44.8±0.1	41.2±0.1	25.6±0.1	54.4±0.2	33.2±0.1	30.5±0.0	33.5±0.1	43.9±0.0
CFA ($K=3$) (<i>f</i>)	45.2±0.1	42.2±0.1	25.7±0.1	55.6±0.1	34.1±0.1	31.2±0.1	33.9±0.0	44.6±0.0
CFA ($K=5$) (<i>h</i>)	44.8±0.0	41.1±0.0	25.6±0.1	54.3±0.2	33.2±0.1	30.6±0.0	33.6±0.1	43.9±0.0
CFA ($K=5$) (<i>f</i>)	51.4±0.4	50.6±0.7	28.3±0.3	69.2±1.3	43.9±0.2	38.9±0.2	38.4±0.2	52.3±0.1

Table 18: Detailed experiment results of Table 5 (Top-1 error rate). (*h*): Hidden representation is normalized before calculating statistics. (*f*): Hidden representation is not normalized.